Nanoscale Advances

ROYAL SOCIETY OF CHEMISTRY

MINIREVIEW

View Article Online
View Journal | View Issue



Cite this: *Nanoscale Adv.*, 2021, **3**, 2679

# Gold nanomaterials for optical biosensing and bioimaging

Peng Si,[a] Nasrin Razmi,[b] Omer Nur,[b] Shipra Solanki,[cd] Chandra Mouli Pandey,[d] Rajinder K. Gupta,[d] Bansi D. Malhotra,[c] Magnus Willander*[b] and Adam de la Zerda*[a]

Gold nanoparticles (AuNPs) are highly compelling nanomaterials for biomedical studies due to their unique optical properties. By leveraging the versatile optical properties of different gold nanostructures, the performance of biosensing and biomedical imaging can be dramatically improved in terms of their sensitivity, specificity, speed, contrast, resolution and penetration depth. Here we review recent advances of optical biosensing and bioimaging techniques based on three major optical properties of AuNPs: surface plasmon resonance, surface enhanced Raman scattering and luminescence. We summarize the fabrication methods and optical properties of different types of AuNPs, highlight the emerging applications of these AuNPs for novel optical biosensors and biomedical imaging innovations, and discuss the future trends of AuNP-based optical biosensors and bioimaging as well as the challenges of implementing these techniques in preclinical and clinical investigations.

Received 16th November 2020
Accepted 12th March 2021

DOI: 10.1039/d0na00961j

rsc.li/nanoscale-advances



## 1. Introduction

Biological sensing and imaging are becoming increasingly important techniques for disease diagnostics and management due to their non-invasiveness, near real time feedback, high accuracy and reliability. Optical biosensing enables continuous monitoring of key health metabolites using wearable and hygienic devices. Optical imaging provides high-resolution images and does not require the use of radioactive contrast agents. These two techniques are further empowered by the development of nanotechnology, which significantly enhances their sensitivity, contrast, specificity and multiplexibility. Gold nanoparticles (AuNPs) are some of the most investigated nanotechnological tools for optical biosensing and bioimaging due to their easy fabrication, chemical stability, outstanding biocompatibility and versatile

[a]*Department of Structural Biology, Stanford University, California, 94305, USA. E-mail: adlz@stanford.edu*
[b]*Department of Science and Technology, Physics and Electronics, Linköping University, SE-60174, Norrköping, Sweden. E-mail: magnus.willander@liu.se*
[c]*Department of Biotechnology, Delhi Technological University, Shahbad Daulatpur, Delhi 110042, India*
[d]*Department of Applied Chemistry, Delhi Technological University, Shahbad Daulatpur, Delhi 110042, India*

*Peng Si is currently a research scientist in Stanford University School of Medicine. He finished his postdoctoral training in Molecular Imaging Program at Stanford and received his PhD in Bioengineering from Nanyang Technological University, Singapore. His current research focuses on developing nanoscale contrast agents and molecular imaging methods for optical coherence tomography. He has published 16 peer-reviewed journal articles (12 first-authored) with over 1200 citations. He received World Molecular Imaging Congress Travel Award in 2017–2019.*

*Nasrin Razmi is an Aquasense Marie Curie Early Stage Researcher and a PhD student in Materials Science at Linkoping University, Sweden. Her main research interest centers around electrochemical sensors. She received her Master's degree in Biology-Biochemistry, and she holds a Bachelor's degree in Cell and Molecular Biology-Biochemistry.*

optical properties. By engineering the shape and size of AuNPs, one can tune many optical properties of AuNPs including localized surface plasmon resonance (LSPR), ratio between light absorption and scattering coefficients, surface enhanced Raman scattering (SERS), fluorescence, *etc.* To date, researchers have fabricated dozens of Au nanostructures, including nanospheres (AuNS),[1] nanorods (AuNR),[2–4] nanoshells (AuNSh),[5–12] nanoprisms (AuNPr),[13–15] nanopyramids (AuNPy),[16] nanobipyramids (AuNBP),[17–19] nanocages (AuNC),[20–25] nanorings (AuNRg),[26–29] nanodisks (AuND),[22,30] nanostars (AuNSt),[31,32] nanorice,[33] nanobowls,[34] nanocrescents (AuNCr),[35,36] *etc.* (Fig. 1), each of which offers unique optical properties. In this article, we provide an overview of recent advances in optical biosensing and bioimaging techniques, which are enabled or enhanced by the unique optical properties of Au nanostructures. We focus on discussion of emerging biosensors and biomedical imaging which leverage the unique LSPR, SERS and luminescence properties of various gold nanomaterials (Fig. 2).

*Chandra Mouli Pandey received his PhD in Chemistry from Banaras Hindu University, Varanasi, in collaboration with CSIR-National Physical Laboratory, New Delhi, in 2015. He is presently working as a DST-INSPIRE Faculty at the Department of Chemistry, Delhi Technological University, Delhi, on the development of biosensors for cancer biomarker detection. He has published more than 30 research papers in international journals and has recently authored a book entitled Biosensors: Fundamentals and Applications. His main research interest is the development of biosensors for health care based on nano-materials, self-assembled monolayers, conducting polymers and bio-nanocomposites.*

*Bansi D. Malhotra received his PhD from the University of Delhi, Delhi, in 1980. He has published more than 324 research papers in refereed international journals, has filed 12 patents, and has co-authored text books on "Nanomaterials for Biosensors: Fundamentals and Applications" and "Biosensors: Fundamentals and Applications". He is a recipient of the National Research Development Corporation Award 2005 for the invention of "Blood Glucose Biochemical Analyzer" and is a Fellow of the Indian National Science Academy, the National Academy of Sciences, India, and an Academician of the Asia Pacific Academy of Materials. His current activities include research and development of nanobiomaterials, biosensors, bio-fuel cells, ordered molecular assemblies, conducting polymers, Langmuir–Blodgett films, self-assembled monolayers, nano biotechnology, biomedical engineering, and biomolecular electronics. He is currently a SERB (Govt of India) Distinguished Fellow and Adjunct Professor at the Department of Biotechnology, Delhi Technological University, Delhi, India.*

*Magnus Willander is a professor (emeritus) in Linköping University and was earlier a professor in Gothenburg University, Sweden. He is an expert on nanomaterials and nanodevices including sensors. He has led several international projects, got several awards and published numerous scientific studies in his field.*

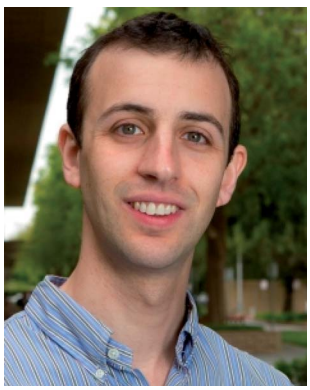

*Adam de la Zerda is an Associate Professor in the departments of Structural Biology and Electrical Engineering at Stanford University. He is working on the development of new cancer imaging technologies. He has received numerous awards including Forbes Magazine 30-under-30, Chan-Zuckerberg Biohub Investigator, Pew-Stewart Scholar, US Air Force Young Investigator Award, Dale F. Frey Award, NIH Director's Early Independence Award, Damon Runyon Fellowship, and Young Investigator Award at the World Molecular Imaging Congress. He has published over 35 papers in leading journals. He is the founder of a medical diagnostics start-up currently in stealth-mode called Visby Medical.*

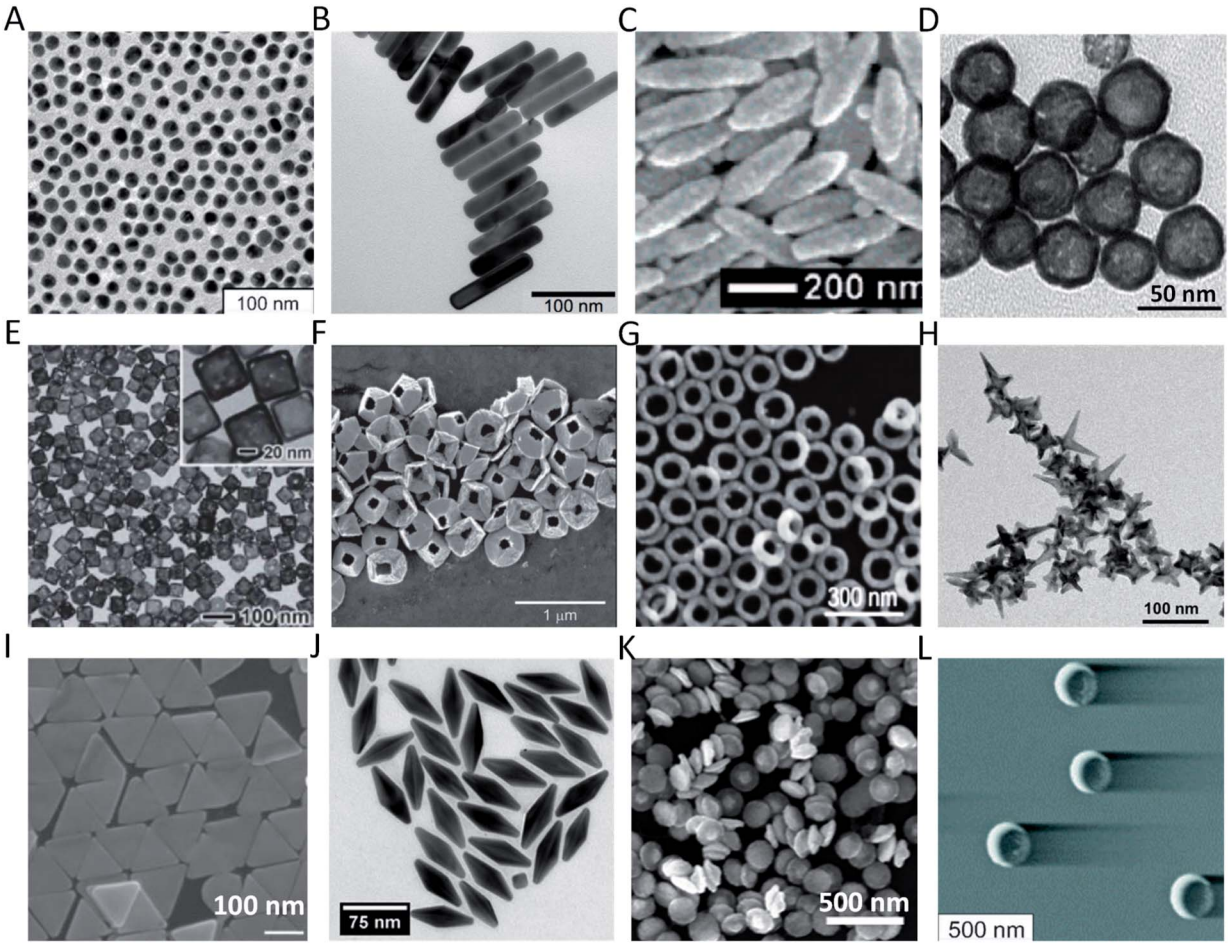


Fig. 1 Au nanostructures of different shapes and sizes with potential applications in optical biosensing and bioimaging: (A) 16 nm AuNS;[1] (B) AuNR;[3] (C) Au nanorice;[33] (D) AuNSh;[11] (E) AuNC;[25] (F) tipless AuNPy;[16] (G) AuNRg;[29] (H) AuNSt;[32] (I) AuNPr;[13] (J) AuNBP;[17] (K) AuND;[22] and (L) AuNCr.[35] Figures are adapted from references with permission. Copyright (2003, 2006, 2007, 2011, 2017) American Chemical Society. Copyright (2009) Elsevier Ltd.

## 2. Optical imaging and sensing based on the LSPR of AuNPs

### 2.1 Optical biosensing based on LSPR shift

Compared to other metal nanoparticles exhibiting LSPR, AuNPs have been found to be the most suitable due to their non-reactive nature and cost-effectiveness. AuNP-based biosensors designed by utilizing this property can be categorized into two different types: one relates to analysis of target analytes based on colorimetric methods developing color due to the aggregation of nanoparticles, and the other utilizes the change in the refractive index of AuNPs for detection.[37] The former assay requires a colloidal solution of AuNPs, whereas the latter method is based on a single AuNP which is usually mounted on a substrate.

AuNP-based colorimetric bioassays are some of the most successful optical biosensors as they involve fewer steps for detection and have also been commercialized. They are based on the wavelength shift caused by changes in interparticle distance.[38,39] The most common example is the pregnancy test kit in which specific antibody-coated nanoparticles show pink color on aggregation upon mixing with a solution containing the particular hormone.[40] Improved sensitivity and selectivity have been achieved by modifying AuNPs with other nanomaterials to make composites because the key objective in these assays is to control the inter-particle forces to manage aggregation. These types of assays are very simple and do not require any sophisticated instrumentation, and thus can be conveniently merged with smartphone imaging to make digital monitoring suitable for near-patient testing platforms.[41,42] A microfluidic colorimetric biosensor for *E. coli* detection based on AuNP aggregation was demonstrated by Zheng *et al.*[42] It was based on HRP + $H_2O_2$ + tyramine (Fig. 3). The device consisted of two mixing channels, one separation channel and a detection channel. Magnetic nanoparticle-modified *E. coli* capture antibodies, detection antibodies, catalase and a sample containing *E. coli* were first introduced into mixing channel 1. The magnetic nanoparticle-tagged bacterial conjugates containing the catalase enzyme were separated in the separation chamber. These bacterial conjugates were then mixed with hydrogen peroxide solution and then mixed with AuNP solution and

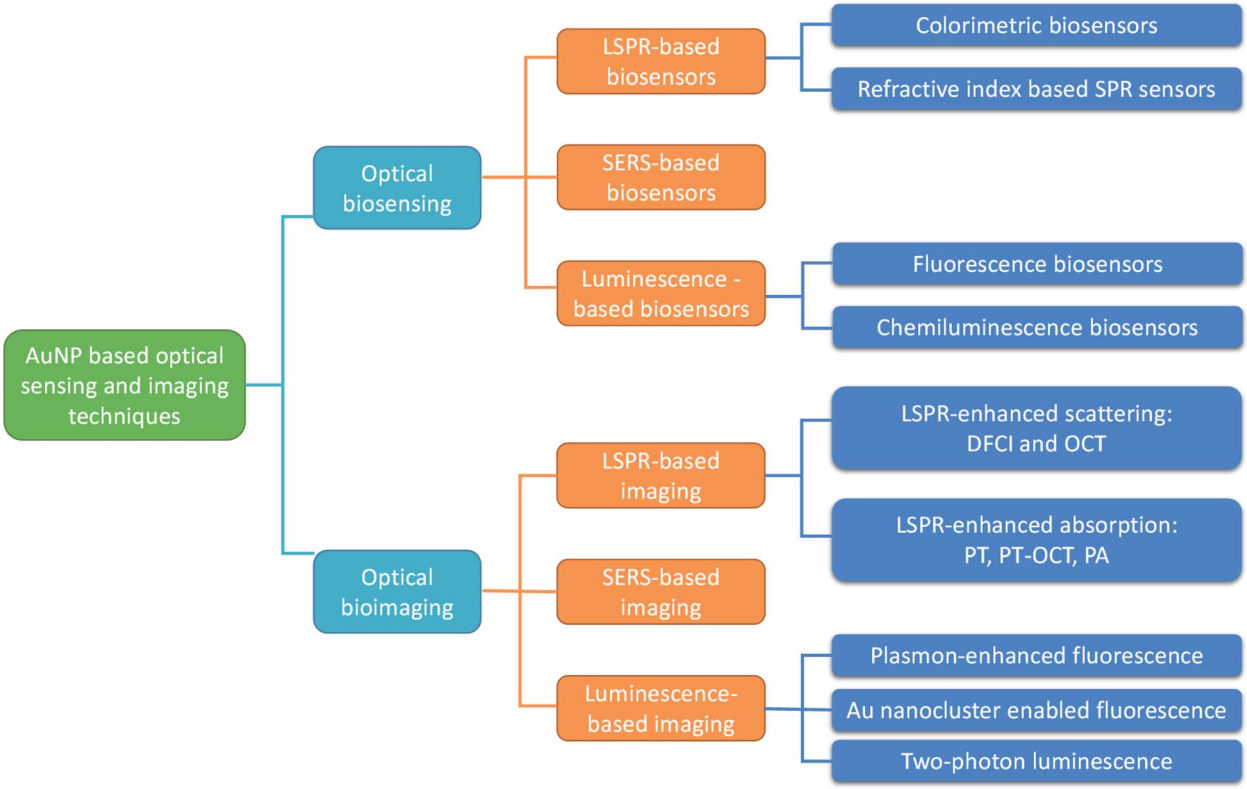


Fig. 2 Various optical biosensing and bioimaging techniques based on AuNPs.

crosslinking agents in the second mixing channel. The phenolic hydroxyl moieties resulted in the aggregation of AuNPs and color change from blue to red (Fig. 3B). Dynamic light scattering studies showed that the size of AuNPs changed from ~13 nm before aggregation to ~670 nm after aggregation and UV-visible studies showed that the aggregated AuNPs showed an absorption peak at 630 nm. This color change was detected using an app on a smart phone. Similarly, in another attempt to exploit the color changing property of AuNPs upon aggregation, a cysteine detection biosensor was designed in which the cysteine functionalized AuNPs did not form aggregates and thus no change in color occurred (Fig. 3C and D).[43]

Recent successes in the field of biosensors influenced by other fields have led to improved investment in colorimetric assays for point-of-care diagnostics.[44] Still, there remains the major challenge of avoiding non-specific aggregation triggering a color change in high ionic strength samples, including serum and urine. Other issues of concern include sample pretreatment requirements and lack of integration with other platforms. These limitations must be resolved and new strategies need to be developed to investigate different designs of AuNP-based biosensors.[45] Assembly-induced or aggregation-based colorimetric assays were developed and widely used for nucleic acid detection by the Mirkin research group.[46–48] They used AuNPs of size ~13 nm with an absorption band from 519–524 nm to tag single stranded DNA fragments and upon hybridization the decrease in distance between the AuNPs resulted in a color change. For example, the color of the solution containing unhybridized DNA was red and upon hybridization the color changed to blue due to the aggregation of AuNPs.[47] In another attempt, two different DNA sequences were identified on a single glass slide array.[48] Two different DNA fragments functionalized with ~50 nm and ~100 nm AuNPs were made for hybridization with probe DNA immobilized on the designed array and the color change occurring due to the aggregation of AuNPs was observed. The DNA fragments tagged with 50 nm AuNPs showed green color at a maximum absorption wavelength of 542 nm on the array after the hybridization event and the other tagged with 100 nm AuNPs showed orange color with a maximum absorption wavelength of 583 nm. Thus, the single array was able to differentiate between two different DNA fragments. In addition to nucleic acid detection, colorimetric sensors are among the most popular and the simplest methods designed for microbial detection. Bui and coworkers[49] reported a highly sensitive colorimetric immunoassay (without enzyme) based on plasmonic AuNPs of size 15 ± 2 nm conjugated to cysteine-loaded liposomes. A chemical cascade reaction due to the presence of a pathogen in the sample caused a visible color shift from red with an absorption peak at 520 nm to dark blue with two bands at 520 nm and 650 nm. The breakdown of cysteine-loaded nanoliposomes due to the presence of the microbes in the sample caused the aggregation of gold nanoparticles, resulting in a visible color change and pathogen detection. The fabricated sensing system was capable of visually detecting single cells of *Listeria*, *E. coli* 0157 and salmonella. In another study, Li and colleagues[50] proposed a visible

 

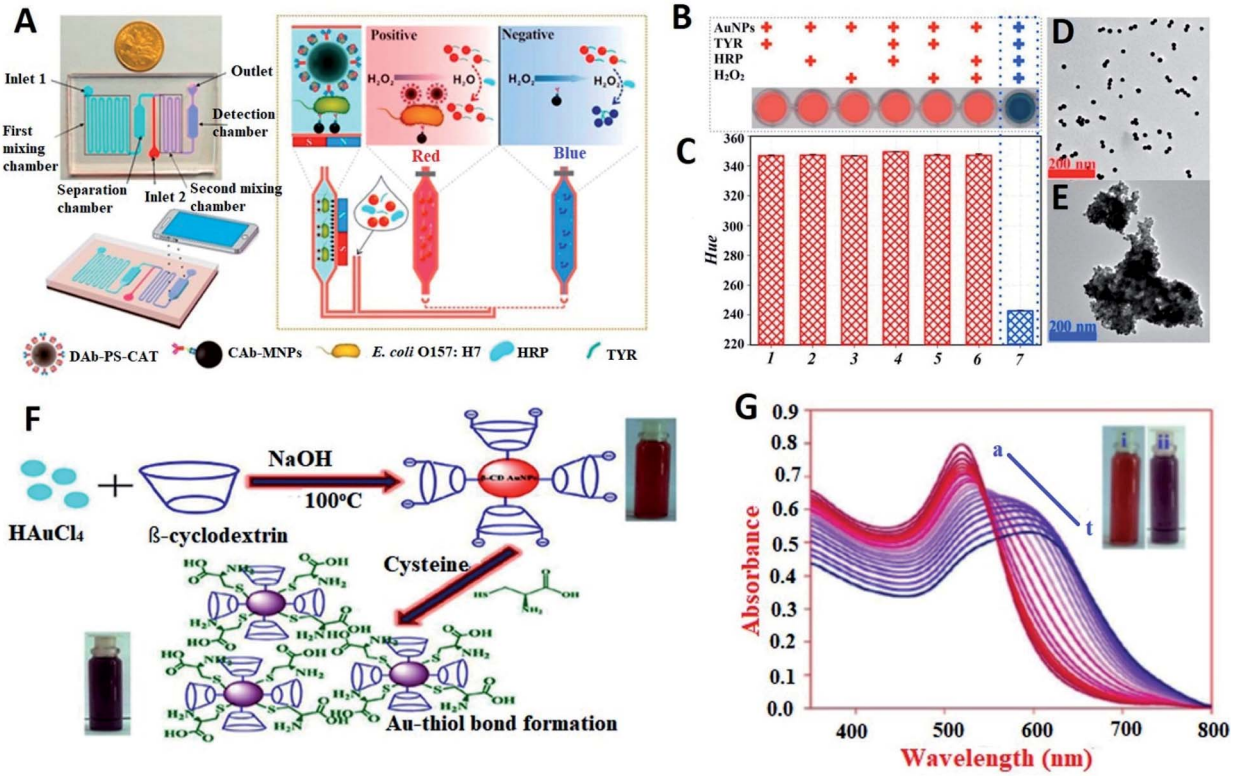


Fig. 3 AuNP-based optical biosensors. (A–E) A smartphone-based biosensor for colorimetric detection of *E. coli* O157:H7. (A) General schematic of the functioning of the biosensor; (B) results of mixing AuNPs with different combinations of cross-linking agents; (C) hue of the mixtures of the AuNPs with different combinations of cross-linking agents; (D) TEM image of the AuNPs before aggregation; (E) TEM image of the AuNPs after aggregation. Figures have been adapted from ref. 42 with permission from Elsevier, copyright 2019. (F and G) A AuNP-based Cys detection biosensor; (F) working principle of the biosensor and (G) SPR band intensity changes for β-CD AuNPs in the presence of incremental addition of Cys (the inset shows the digital images of β-CD AuNPs in the absence (i) and presence (ii) of Cys). Figures have been adapted from ref. 43 with permission from the Royal Society of Chemistry, copyright 2020.

colorimetric sensor using AuNPs with various surface charges allowing fast and differential response to 15 pathogens with different surface electronic properties in five seconds. A specific color shift pattern due to the interaction of gold nanoparticles and microorganisms was obtained for each of the microorganisms. The advantages of the proposed sensor are its simplicity, rapidness, and visual and label free detection. In addition, the proposed sensor is applicable in environmental monitoring and clinical diagnostics. Recently You *et al.*[51] fabricated a visual colorimetric nitrocellulose membrane strip-based sensing assay for Gram positive bacteria by using vancomycin-modified gold nanoparticles and one-pot reaction. They took advantage of the broad spectrum inhibiting activity against Gram-positive bacteria of the vancomycin antibiotic and 9.5 nm spherical AuNPs. The assay could differentiate between Gram-negative and Gram-positive bacteria. The obtained detection limits with the naked eye for all Gram-positive *S. aureus*, *M. luteus*, and *B. subtilis* were $1 \times 10^9$ cells per mL, and there was no interaction of the synthesized complex with Gram-negative bacteria such as *E. coli*. The proposed sensing array was able to detect *S. aureus* in tap water and orange juice.

Refractive index-based biosensors utilize the fact that the LSPR of AuNPs is sensitive to the changes near their surface, enabling them to monitor the biomolecular interactions with ultrahigh sensitivity. This is a label-free technique compared to the colorimetric assays. It has the advantage of preserving the structures of biomolecules and has been utilized to study the complete reaction kinetics and protein interactions. The plasmon resonances of different Au nanostructures have been evaluated to improve the performance and sensitivity of SPR assays. Even the amplification of SPR signals has been demonstrated by utilizing the coupling of LSPR of AuNPs with the propagating SPR signal of Au films leading to enhanced incident angle shift and higher sensitivity.[52] Active research is being conducted by different research groups to bring this technology to the market. However, challenges such as improvement in sensitivity, selectivity, detection limit, detection time and multiplexing capabilities need to be addressed. Using dark field microspectroscopy, Nusz and coworkers demonstrated that gold nanorods of dimensions 74 ± 9 nm (length) and 33 ± 6 nm (diameter) conjugated with biotin can detect streptavidin molecules at a sensitivity of 1 nM.[53] It is also possible for the system to detect serum proteins with nanomolar sensitivity.[54] The wavelengths studied in both the cases range from 700 to 800 nm. The readers can refer to the review article published by Hafner *et al.*[55] for more details regarding LSPR refractive index sensors. Here we focus on applications of this technique for bacteria detection. LSPR-based refractive index sensors have been used as a real time and rapid

methodology for bacteria detection by using different types of bioreceptors. However, in some measurements, interference of bacteria size can affect the detection limit, and in some cases, large size, high cost, complexity of the method and false result due to the effect of the composition of the sample or temperature, which causes refractive index fluctuations, are the disadvantages of SPR. Vaisocherová-Lísalová and coworkers constructed a rapid, sensitive and simultaneous SPR-based biosensor using streptavidin-coated gold nanoparticles and based on ultralow fouling and functionalizable poly(-carboxybetaine acrylamide) (pCBAA) brushes for multi-step detection of microorganisms in complex food samples. The proposed assay was composed of the following three steps: (i) crude food samples for sensor incubation, (ii) binding of secondary biotinylated antibodies, and (iii) binding of streptavidin-coated gold nanoparticles to the biotinylated antibodies. Limits of detection of $7.4 \times 10^3$ CFU per mL and $11.7 \times 10^3$ CFU per mL for *Salmonella* sp. and 57 CFU per mL and 17 CFU per mL for *E. coli* in cucumber and hamburger extracts were achieved.[56] Zhou *et al.* recently reported a biosensor based on nanogold enhanced surface plasmon resonance and colloidal gold test strips (ICTS) for *Vibrio parahaemolyticus* detection.[57] The response for the pathogen was improved dramatically after immunomagnetic separation.

### 2.2 Optical imaging based on LSPR-enhanced scattering

The scattered light intensity of AuNPs is about $10^5$ to $10^6$ times stronger than that of a fluorescein molecule and 100–1000 times stronger than that of a polymer bead.[58–60] Larger AuNPs show stronger scattering efficiencies than smaller AuNPs.[59] In contrast to fluorophores, light-scattering AuNPs are not photobleachable which makes them very attractive contrast agents for bioimaging. In this section, we focus on two imaging modalities which detect the backscattering of AuNPs: dark field confocal imaging (DFCI) and optical coherence tomography (OCT). DFCI is often used for *in vitro* imaging of cells and biomolecules and OCT is commonly used for *in vivo* imaging.

DFCI can detect AuNPs that are as small as 10 nm in diameter. Using a dark field microscope with a high NA lens, light scattered from AuNPs can be imaged as bright spots even though the dimensions of AuNPs are smaller than the diffraction limit of the lens. A major advantage of DFCI is that it allows high-contrast, true-color and multiplexed detection of gold nanoparticles with different sizes and shapes. Various types of AuNPs including AuNS, AuNR, AuNC and AuNSh have been implemented as DF optical contrast agents for cancer cell imaging by functionalizing their surface with ligand binding to cell surface receptors (Fig. 4).[61–65] AuNPs are also extensively utilized as DF probes to image a variety of intracellular biological processes such as cell division, endocytosis, virus infection, DNA damage, *etc.* For example, Qian *et al.* applied bioconjugated AuNS and DF imaging to track cell division in real time.[66] Wan and co-workers were able to label AuNPs on respiratory syncytial virus and visualize its infection of HEp-2 cells.[67] These studies have provided many new insights into intracellular events.

OCT is an interferometry-based imaging technique which illuminates samples with near-infrared (NIR) low-coherence light and detects the back-scattered light from samples. Intuitively, AuNPs are attractive OCT contrast agents because they

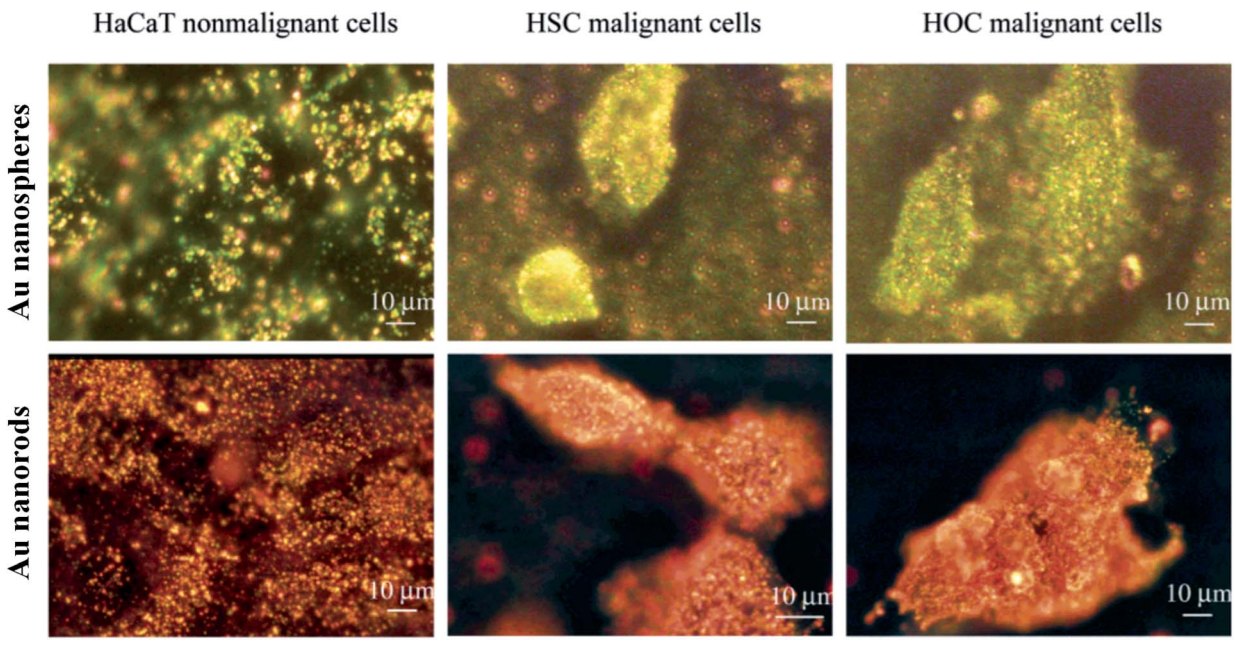


Fig. 4 Dark-field microscopy images of normal and two different types of cancer cells after incubating with AuNS/AuNR conjugated with anti-EGFR antibodies. AuNS show green to yellow color in the dark-field image (upper panel), indicating that their light scattering is mostly in the visible region. AuNR show orange to red color in the dark-field image (lower panel), indicating that their light scattering is mostly in the NIR region. Modified and reprinted with permission from ref. 156. Copyright (2006) American Chemical Society.

Table 1 Optical properties and optical imaging applications of different types of gold nanoparticles[a]

| Au nanostructure | Fabrication method | LSPR (visible: 400–700 nm, NIR-I: 700–1000 nm, NIR-II: 1000–1700 nm) | Optical imaging modalities/ applications |
|---|---|---|---|
| Nanoshell | Overgrowth of core-bound particles[157] | NIR-I–NIR-II | OCT[5–10]<br>PA[11,12] |
| Nanorod | Seeded growth with CTAB[158] | Visible–NIR-II | OCT[3,4,68–74]<br>PA[99–104]<br>TP fluorescence[147,148] |
| Nanostar | Seeded growth with CTAB or PVP; one-pot synthesis[159] | Visible–NIR-I | OCT[75]<br>PA[105]<br>SERS[31,32,118]<br>TP fluorescence[149,150] |
| Nanocage | PVP-stabilized polyol, galvanic displacement[160] | Visible–NIR-I | OCT[20–22]<br>PA[23,24] |
| Nanodisk | Nanoimprint lithography[22] | Visible–NIR-I | OCT[21,22] |
| Nanoring | Lithography using colloidal polystyrene nanoparticles as the template[27,28] | NIR-I–NIR-II | OCT[26,28] |
| Nanobipyramid | Seeded growth with CTAB and CTAC[17] | Visible–NIR-II | OCT[18,19]<br>SERS[124,125] |
| Nanoprism | Seeded growth with CTAB[13] | NIR-I–NIR-II | OCT[14,77,161] |
| Nanopyramid | Lithography with patterned photoresist posts as the template[16,162] | Visible to NIR-I | SERS[16] |
| Nanocrescent | Lithography with a nanosphere template and vapor-phase deposition[35,36] | Visible to NIR-II | SERS[36,120] |
| Nanoclusters | Alkanethiol/phosphine-stabilized reduction[163] | Visible to NIR-I | Fluorescence[142–146] |

[a] CTC: circulating tumor cells, OCT: optical coherence tomography, SERS: surface enhanced Raman scattering, TP: two-photon, NIR: near infrared, CTAB: cetyltrimethylammonium bromide, CTAC: cetyltrimethylammonium chloride; PVP: poly(vinylpyrrolidone).

can enhance the backscattering of light at a specific wavelength due to LSPR. LSPR also generates drastic difference in the intensity of backscattered light at different wavelengths, allowing different AuNPs to have unique spectral signatures. Due to their highly tunable plasmonic resonances and scattering coefficient, AuNPs of different shapes and dimensions have been extensively investigated as OCT contrast agents in recent years. AuNSh,[5–10] AuNR,[3,4,68–74] AuNSt,[75] AuNC,[20–22] AuNRg,[26,28] AuND,[21,22] AuNPr[14,15,76,77] and AuNBP[18,19] have been demonstrated to be promising contrast agents to improve OCT signals in tissue and blood vessels (Table 1). Among them, AuNSt, AuNC and AuND have plasmonic resonance peaks mainly in the first near infrared window (NIR-I, 700–1000 nm) so they are used as contrast agents for OCT with a light source in the NIR-I region; while AuNR, AuNSh, AuNRg, AuNPr and AuNBP can be employed as OCT contrast agents in both NIR-I and NIR-II windows. There are two commonly used methods to synthesize AuNPs as OCT contrast agents: nanolithography methods are used to fabricate gold nanodisks and nanorings, whereas seed-mediated growth is used to fabricate AuNPs of other geometries. The advantage of the nanolithography method is that it can fabricate AuNPs with precise dimensions with small variation in size, but it is expensive, time consuming and difficult to scale up the fabrication. In contrast, wet chemistry methods are low-cost, efficient and easy to scale up, but may have higher dimension variation and impurity.

AuNR are some of the most heavily investigated AuNPs as OCT contrast agents due to their highly tunable size and aspect ratio and facile preparation method. Their plasmonic resonance can be tuned from 600 to 1300 nm by adjusting their aspect ratio, and the scattering to absorption cross-section ratio can be changed by adjusting their size.[59,78] SoRelle *et al.*[3,4] showed that AuNR with larger dimensions (90 × 30 nm) exhibit 30-fold greater backscattering or OCT intensity than AuNR with a smaller size (50 × 15 nm). In addition, they show that two types of AuNR with different plasmonic resonances, 815 nm and 925 nm, can be used as spectral contrast agents and detected multiplexably by OCT. The AuNR spectral OCT contrast agents were then implemented for retinal imaging,[72] tracking of brain tumor-associated macrophages[79] and detecting circulating tumor cells.[80] Ratheesh *et al.*[71] demonstrated that AuNR with a higher aspect ratio of 8.8 and a plasmon-resonance peak at 1320 can be used as contrast agents to enhance OCT imaging in the 1300 nm range. Lippok and co-workers[73] demonstrated for the first time that AuNR can depolarize the backscattered OCT light and the depolarization signature of AuNR can be well detected in biological tissue.

AuNPr have been increasingly investigated as OCT contrast agents in recent years. Si *et al.* synthesized AuNPr with high scattering cross-section and LSPR in the NIR-II window, and demonstrated that intravenous injection of AuNPr can dramatically enhance the contrast of OCT vascular imaging,

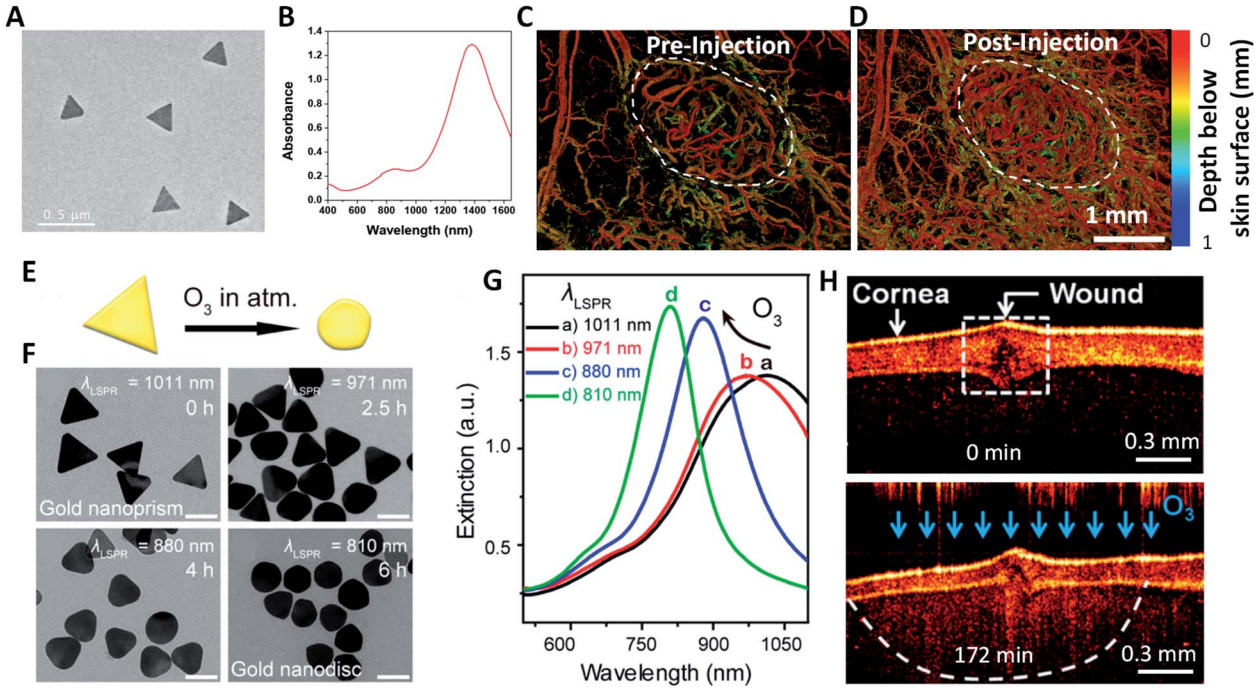


Fig. 5 AuNPr as OCT contrast agents for contrast enhanced vascular imaging and ozone sensing. (A and B) TEM image and extinction spectrum of AuNPr which have strong plasmonic scattering in the NIR-II region. (C and D) The OCT angiograms of a melanoma tumor implanted on a mouse ear before and after systematically injecting the NIR-II AuNPr. Reprinted with permission from ref. 14. Copyright (2018) American Chemical Society. (E–G) Geometric and plasmonic evolution of AuNPr upon exposure to ozone ($O_3$). Upon exposure to $O_3$, the corners of AuNPr are gradually rounded and the LSPR of AuNPr exhibits a blue shift accordingly. (H) OCT images of a AuNPr-infiltrated crucian carp eye before and at 172 min post exposure of 75 ppm $O_3$. Reprinted with permission from ref. 15. Copyright (2017) American Chemical Society.

especially for tumors (Fig. 5A–D).[14] Zhou and co-workers demonstrated that AuNPr can be used for three-dimensional (3D) ozone imaging in the anterior chamber of an isolated crucian carp eye.[15] Upon exposure to $O_3$, AuNPr transform their shape gradually into circular nanodiscs, resulting in a blue shift of their plasmon-resonance peak from 1050 nm to 830 nm (Fig. 5E–G). Using an OCT system with the center beam wavelength at 830 nm, $O_3$ can be sensitively detected due to the strong OCT intensity signals from gold nanodiscs (Fig. 5H). In another study, Zhou *et al.* synthesized a nanohybrid AuNPr@-polyaniline core–shell structure, which can reversibly change its extinction and scattering properties at 830 nm under different acidic and basic conditions.[77] The AuNPr@polyaniline was employed as an OCT contrast agent to dynamically image the pH distribution in the anterior chamber of a fish's eye.

### 2.3 Optical imaging based on LSPR-enhanced absorption

Both photothermal (PT) and photoacoustic (PA) imaging take advantage of AuNPs' strong light absorption at their plasmon resonance peak. AuNPs produce heat upon absorbing laser light at their plasmon-resonance wavelength, which results in refractive index change of the surrounding medium and elastic expansion in the surrounding air. PT imaging relies on the detection of phase shift of the transmitted light beam caused by refractive index change, while PA imaging is based on detecting the acoustic waves generated by air expansion. In contrast to AuNP contrast agents, which usually have sizes above 30–40 nm, used for scattering-based imaging techniques, AuNPs suited for PT and PA imaging are much smaller in dimension, and have higher absorption-to-scattering cross-section.

PT imaging was first reported by Boyer and coworkers,[81] who used a green laser to focus on the sample where AuNPs absorb the light and produce heat. Another red laser beam is split into two orthogonally polarized beams, one of which focuses on the same point as the green laser. The red laser beams reflected from the sample are then recombined and the relative phase change is identified using a detector. They show that such a technique can sensitively image gold nanospheres as small as 10 nm in diameter. Berciaud *et al.* further demonstrated that PT imaging can detect even 1.4 nm AuNPs consisting of just 67 atoms, and measure the absorption spectra of individual AuNPs with diameter down to 5 nm.[82] Zharov *et al.* applied AuNPs[83–85] and Au-coated carbon nanotubes[86,87] as PT imaging contrast agents to visualize adherent and circulating cancer cells, circulating stem cells and lymphatic vessels. Further, these researchers demonstrated super-resolution PT microscopy based on non-linear dependence of signals on laser energy, with a 50 nm spatial resolution.[88]

Photothermal OCT (PT-OCT) combines PT-imaging and OCT to allow high-sensitivity and high-contrast *in vivo* imaging. The PT laser source is coupled to the sample arm of the OCT system, exciting the contrast agents that are within the optical path length of the OCT beam. Upon excitation, the photothermal effect of the contrast agents changes the

 

temperature of their surrounding environment and causes a variation of the local refractive index, which leads to an alteration of the optical path length which changes the phase of the backscattered OCT beam. The phase change is then detected by phase-sensitive OCT.[89] Many types of gold nanostructures, including AuNS,[90] AuNSh,[91] and AuNR,[92–97] have been investigated as PT-OCT contrast agents due to their strong absorption cross-section and the resulting photothermal effect. Among them, AuNR are most promising because they are highly efficient in absorbing light and releasing heat. Tucker-Schwartz *et al.*[93] showed that they could image AuNR accumulated in mouse tumor tissue using PT-OCT with very high signal-to-noise ratio. These AuNR were subcutaneously injected and then they accumulated in tumors through the leaky vasculature. Jung *et al.* demonstrated that they can image the concentration and time-dependent uptake of AuNR in sentinel lymph nodes using PT-OCT.[97] Recently, Lapierre-Landry *et al.*[94] and Gordon *et al.*[95] have demonstrated AuNR as PT-OCT contrast agents that can be specifically detected in the retina of laser-induced choroidal neovascularization (LCNV) mouse models after systematic injections. The former study shows that the PT-OCT signals in the LCNV lesion are associated with non-targeted AuNR passively accumulated in the eye, whereas the latter study applies PT-OCT to detect antibody-conjugated AuNR targeting the LCNV lesion. The latter study also investigated the effect of anti-angiogenic treatment in the retina of a LCNV mouse model using targeted AuNR as PT-OCT contrast agents. Notable reduction of PT-OCT signals is detected in the LCNV lesion after intravitreal delivery of neutralizing monoclonal anti-vascular endothelial growth factor (anti-VEGF) antibodies.

PA imaging takes advantage of the high resolution of optical imaging and the deeper tissue penetration of ultrasound imaging. It permits tissue penetration up to 5 cm and spatial resolution up to tens of micrometers. AuNPs that are strong absorbers of NIR light are ideal PA contrast agents as NIR light penetrates deeper in animal tissues. AuNP-based PA contrast agents have been intensively investigated in the past decade for a wide range of preclinical applications, including cancer detection, atherosclerotic plaque imaging, brain function measurements, image-guided therapy, *etc.* Because both PT and PA contrast agents are strong absorbers of NIR light, many AuNPs that are used for PT and PT-OCT imaging can be used for PA imaging, including AuNS,[98] AuNSh,[11,12] AuNR,[99–104] AuNC[23,24] and AuNSt.[105] Although AuNR have been utilized as PA contrast agents for a variety of applications including multiplexed cell tracking,[102] cardiovascular imaging,[100] stem cell imaging[103] and cancer cell detection,[104] regular AuNR have suboptimal thermal stability under a high-intensity pulsed laser used for PA irradiation, leading to plasmonic resonance shift and decay of PA signals over time. In a recent study, Chen *et al.*[2] report that miniature AuNR that are 5–11 times smaller than regular-sized AuNR, are 3-fold more thermally stable and produce 3.5-fold stronger PA signal intensity than their absorption-matched larger counterparts in the NIR-II window (Fig. 6A and B). Upon IV injection of these small targeted AuNR in a tumor-bearing mouse model, they improved the tumor delivery efficiency by 30% and PA contrast by 4.5 times (Fig. 6C and D).

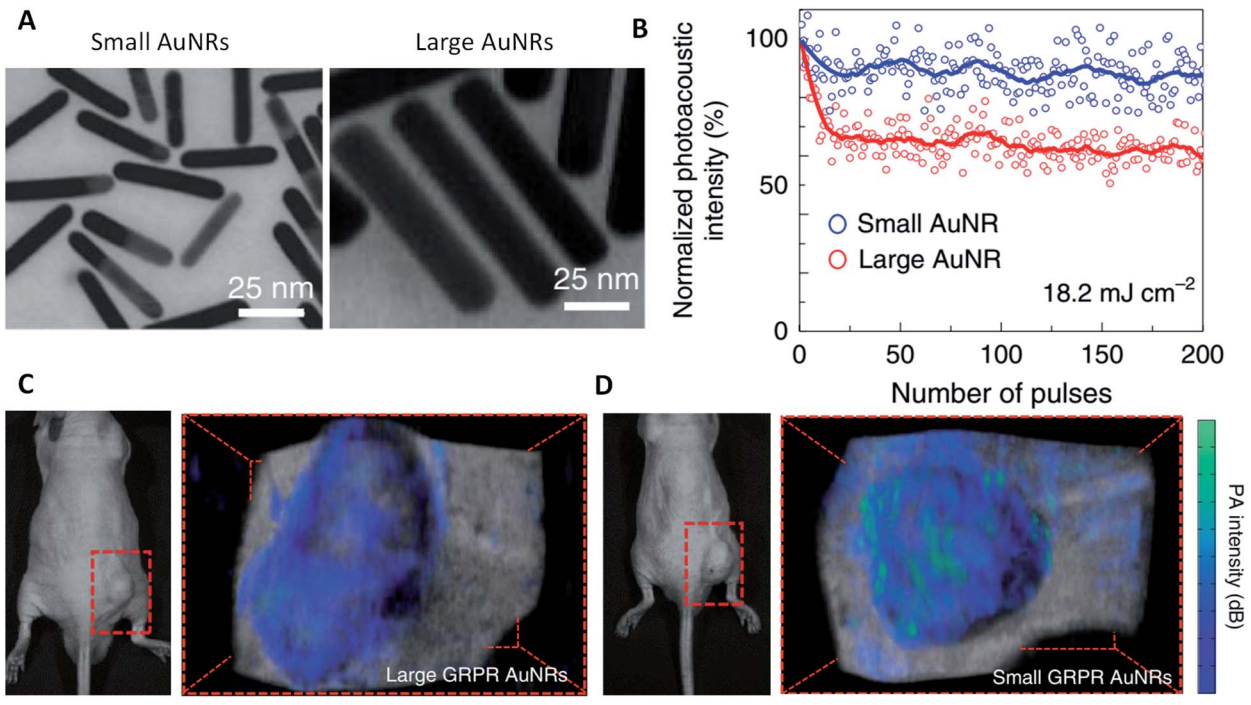


Fig. 6 Small AuNRs enhanced PA imaging. (A) TEM images of small and large AuNRs. (B) PA signal intensities of small and large AuNRs upon illumination with 200 laser pulses at 18.2 mJ $cm^{-2}$. (C and D) PA images of tumor-bearing mice after administration of prostate cancer targeting GRPR peptide-functionalized large and small AuNRs. Reprinted with permission from ref. 2. Copyright (2019) Springer Nature.

## 3. Optical sensing and imaging based on SERS

Though the Raman scattering effect is a very weak phenomenon, a drastic increase in the scattering intensity has been observed when it takes place in the vicinity of AuNPs, a phenomenon called SERS. SERS offers several advantages such as being non-destructive, having potential for multi-component analysis, yielding compound-specific information, and can be performed in the presence of water, making it suitable to study processes *in vivo*.[106]

### 3.1 SERS-based optical sensing

Raman scattering is gaining increased research attention in the field of biosensing because of its single-molecule sensitivity, intrinsically sharp fingerprints, and the availability of a wide range of photo-stable labels. To achieve high sensitivity the SERS signal has to be enhanced by either modifying the surface properties or by increasing the number of molecules generating Raman signal. Monolayer films of AuNPs have discrete physical and chemical properties due to quantum confinement and interparticle coupling.[107] These properties are highly useful in SERS applications. AuNP monolayers with nanogaps have shown an increase in the SERS signal but their surface uniformity hinders the performance.[108] Thus, numerous attempts have been made to fabricate AuNP monolayers with desired density and precisely controlled nanogaps.[109–111] For example, Shao *et al.* fabricated a multiple signal amplification sandwich type SERS biosensor for the detection of miRNA with a detection limit of 3 fM. A triple signal amplification was achieved by using AuNPs of selective morphology, hybridization chain reaction amplification and using silver nanoparticles in combination with AuNPs.[110]

Wang and co-workers[112] developed an interesting SERS-based biosensing platform that is able to differentiate between two different DNA targets simultaneously (Fig. 7). A lateral flow assay was able to detect DNA associated with Kaposi sarcoma-associated herpesvirus (KSHV) and bacillary angiomatosis (BA) (Fig. 7C). The Raman peak intensity centered at 1617 $cm^{-1}$ was monitored, and its variation was used for the quantitative evaluation of KSHV and BA (Fig. 7D).

Currently, there are no SERS-based diagnostic devices in the market, but efforts are being made to reduce the complexity of software and instrumentation to commercialize the products. SERS is very promising for pathogen detection owing to its high sensitivity and selectivity.[113] Some of the commonly used platforms for SERS are nanomaterials such as gold nanostructured

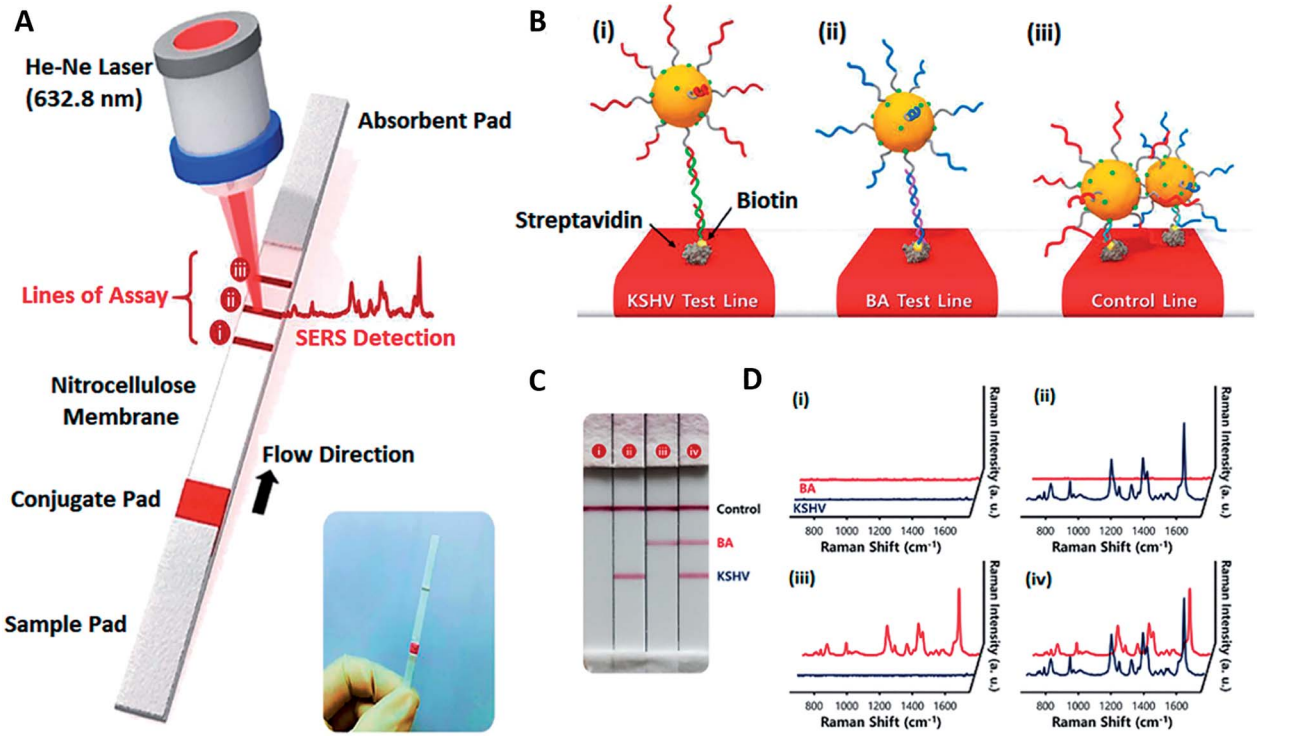


Fig. 7 SERS-based LFA for KSHV detection. (A) Scheme of the LFA biosensor for the simultaneous detection of two nucleic acids. The strip consists of two test lines and one control line. (B) (i) KSHV DNA–Au NP complexes were captured by the probe KSHV DNA on the first test line; (ii) BA DNA–Au NP complexes were captured by the probe BA DNA on the second test line, and (iii) excess KSHV and BA detection DNA attached to AuNPs were captured by control DNA through T20–A20 hybridization on the third control line. (C) Digital photographic images and (D) corresponding SERS spectra of the SERS-based LFA biosensor in the presence of (i) KSHV, 0 pM; BA, 0 pM; (ii) KSHV, 100 pM; BA, 0 pM; (iii) KSHV, 0 pM; BA, 100 pM; (iv) KSHV, 100 pM; BA, 100 pM. Assay time: 20 min. Reprinted with permission from ref. 112. Copyright (2017) American Chemical Society.

surfaces and gold colloidal particles. The Raman scattering from molecules in the vicinity of a gold nanomaterial surface due to the coupling effect of surface plasmon through the oscillating electric field can be described as electromagnetic enhancement. An enhancement factor of $10^6$ to $10^{14}$ is enough to allow the detection of a single target molecule, which makes them highly suitable approaches for the detection of pathogens.[114,115] Mevold and coworkers[116] have conducted a SERS-based study for sensitive bacteria detection by using a graphene–gold nanoparticle nanohybrid. Cationic poly(-diallyldimethylammonium chloride) (PDDA) functionalized graphene nanosheets were prepared. The traditional citrate thermal reduction method was applied to synthesize gold nanoparticles which were electrostatically immobilized onto graphene–PDDA nanohybrid sheets. The result of transmission electron microscopy (TEM) showed that the particle size was 15–20 nm. The zeta potential value of the nanohybrid ratio was 7.7–38.4 mV. The methodology was applied for the detection of *S. aureus* confirming its application in label-free and rapid biosensing of microorganisms and target biomolecules. In another study, Ma and colleagues[117] proposed a rapid and simple SERS-based biosensor for sensitive and selective *Salmonella typhimurium* (*S. typhimurium*) detection using spiny AuNPs functionalized with 4-mercaptobenzoic acid and specific thiolated *S. typhimurium* aptamers as SERS nanoprobes. Under optimal conditions, a low limit of detection of 4 CFU per mL was obtained for the detection of *S. typhimurium*.

### 3.2 SERS-based optical imaging

Compared with other optical imaging modalities, SERS has the advantage of high sensitivity, which allows contrast agents to be detected at a concentration as low as 1.5 fM.[118] In recent decades, SERS imaging agents have been increasingly studied by conjugating Raman active molecules on AuNPs with various structures. These AuNPs can dramatically enhance the Raman signals of dyes conjugated on them by an order of $10^{10}$. AuNPs with rough geometrical features such as sharp tips and edges, commonly known as 'Raman hot spots', can even improve the Raman signals to the order of up to $10^{15}$ fold,[119] because the spatial confinement of the surface plasmons at these 'hot spots' produces a highly concentrated local secondary electromagnetic field. AuNPs with quite a few different morphologies can provide such 'Raman hot spots', including AuNSt,[31,32,118] AuNPy,[16] AuNCr,[36,120] nanourchins,[121–123] AuNBP,[124,125] *etc.* For example, Harmsen *et al.* demonstrated that an AuNSt-based SERS agent can be used to precisely detect macroscopic malignant lesions and microscopic tumor invasion with high sensitivity in animal models of pancreatic cancer, breast cancer, prostate cancer, and sarcoma, and in one human sarcoma xenograft model.[118] In recent studies, Bardhan and coworkers

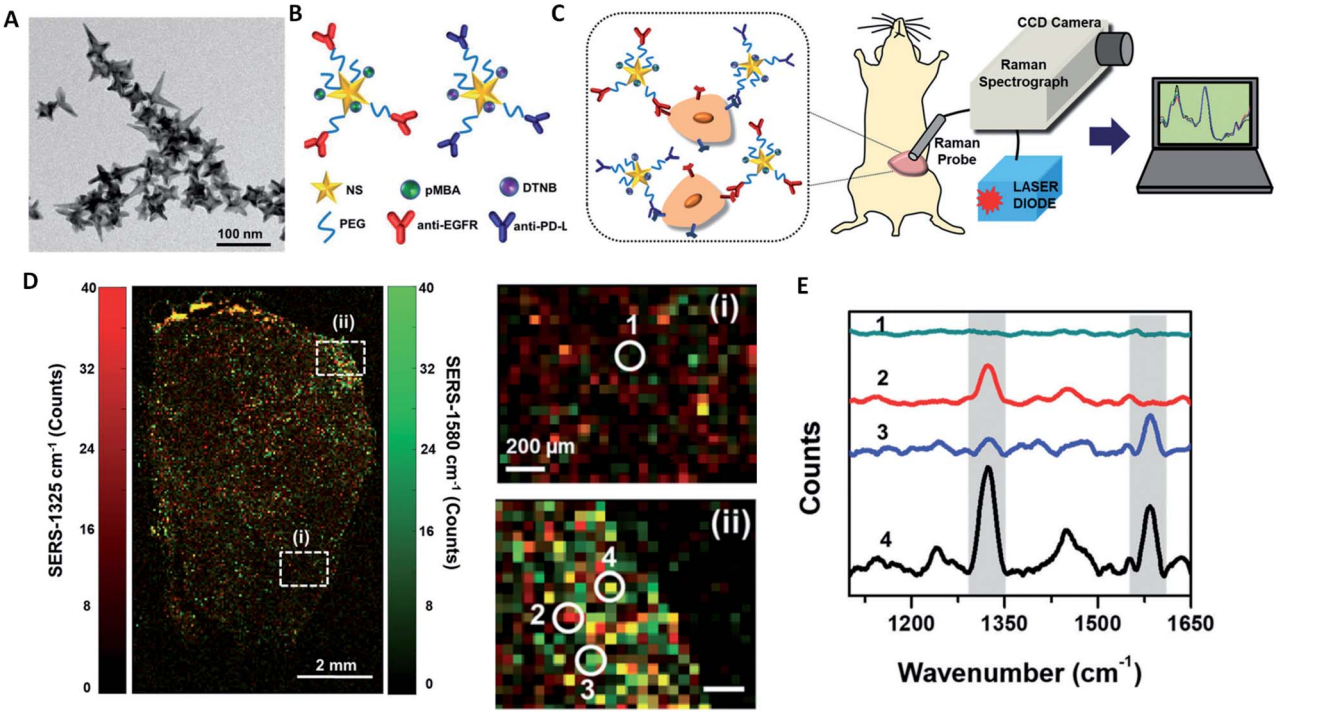


Fig. 8 Multiplexed SERS immunoimaging using AuNSt. (A) TEM images of AuNSt used for SERS. (B) Scheme of AuNSt functionalized with two different Raman-active tag/targeting antibody pairs. The Raman tag pMAB is paired with anti-EGFR, and DTNB is paired with anti-PD-L1. (C) Schematic illustration of the SERS setup for multiplexed tumor immunoimaging. (D) The SERS signals of both DTNB (1325 $cm^{-1}$) and pMBA (1580 $cm^{-1}$) in *ex vivo* mouse breast cancer tissue. Subsection (i) shows a region of interest (ROI) with little AuNSt accumulation, whereas subsection (ii) shows a ROI with rich AuNSt accumulation. (E) The corresponding Raman spectra of ROI (1)–(4) in (D), where (1) shows no AuNSt binding, (2) shows high PD-L1 expression, (3) shows high EGRF expression and (4) shows high expressions of both PD-L1 and EGFR. Reprinted with permission from ref. 32. Copyright (2018) the Royal Society of Chemistry.

reported multiplexed imaging of immuno-biomarkers using AuNSt-based SERS imaging (Fig. 8).[31,32]

# 4. Optical sensing and imaging based on AuNP-induced luminescence

## 4.1 Optical biosensors based on AuNP luminescence

Luminescence-based optical biosensors, in which the detection is carried out *via* either fluorescence or chemiluminescence, offer a variety of advantages such as high selectivity, excellent sensitivity and flexibility.[126] Fluorescence-based biosensors can be of colorimetric type giving visual results using AuNPs' individual fluorescence or fluorescence resonance energy transfer (FRET). Elahi and coworkers proposed a fluorescence biosensor for *Shigella* sp. detection by employing AuNPs.[127] As a signal reporter two DNA probes were immobilized on gold nanoparticles. A third DNA probe was immobilized on SMCC (sulfosuccinimidyl 4-*N*-maleimidomethyl cyclohexane-1-carboxylate) modified iron nanoparticles (MNPs). The DNA probe–AuNP–fluorescence DNA probe and the MNP–DNA probe were added to target DNA. By using a magnet, the MNP–DNA probe–target DNA–DNA probe–AuNP–fluorescence complex was isolated. Fluorescence intensity was studied by fluorescence spectrophotometry after the signal generation when a fluorescence DNA probe was released on the surface of AuNPs. By increasing the target DNA concentration, the fluorescence intensity was increased accordingly. A low detection limit of 102 CFU per mL for *Shigella* sp. was successfully achieved.

Plasmonic AuNPs can interact with different fluorophores resulting in either fluorophore quenching or enhancement also known as FRET. Quantum dots (QDs) and AuNPs are the most commonly used FRET pairs in fluorescence-based optical biosensors due to the overlapping of AuNPs' absorption spectrum with QDs' emission spectrum.[128–130] But the applicability of QD-based FRET biosensors is limited by their high cost, toxicity, the strong dependence of performance on surface states and chemical instability.[131] Metal nanoparticles or metal-doped nanoparticles are emerging as new alternatives of QDs in FRET-based biosensors.[131,132] Zhang *et al.* used amino capped silicon nanoparticles (SiNPs) and citrate capped AuNPs as FRET pairs to design an L-Csyteine (L-Cys) biosensor.[131] In the fabricated biosensor, fluorescence quenching of SiNPs with AuNPs and the restoration of fluorescence by the addition of L-Cys due to the release of AuNPs from the SiNP–AuNP complex have been demonstrated. The intensity of fluorescence restored is directly proportional to the concentration of L-Cys added. FRET-based biosensors possess many advantages such as real-time monitoring, visual monitoring, being capable of multiple analyte detection *etc.* Despite various merits, there are some demerits such as the cost of FRET reagents, selection of fluorophores, stability of functionalized nanoscale materials, low fluorescence resolution and low signal-to-noise ratio.

Electrochemiluminescence (ECL) or electron generated chemiluminescence based biosensors are emerging and less explored categories of biosensors which are gaining increasing attention. These are based on the phenomenon in which the luminescent species absorb energy from the electrochemical reaction occurring near their surface. AuNPs have been extensively used in ECL-based biosensors for signal amplification.[133–135] An ultrasensitive ECL biosensor for exosome detection was developed using recently discovered two-dimensional nanomaterials MXenes and AuNPs.[135] In this work, a glassy carbon electrode was modified with exosome specific aptamers and then attached to the target exosomes derived from HeLa cells. Then aptamer conjugated MXenes were attached to the modified electrode, followed by immersion in $HAuCl_4$ for *in situ* synthesis of AuNPs. The MXenes acted both as stabilizers and reductants, and the *in situ* formed AuNP–MXene hybrid not only demonstrated highly efficient recognition of exosomes but also provided a large catalytic surface with AuNPs. A 1000 times lower detection limit (*i.e.* 30 particles per μL) than that of the conventional ELISA was achieved. These ECL biosensors are highly advantageous in terms of specificity as the signal is due to the biorecognition reaction.

## 4.2 Optical imaging based on AuNP luminescence

AuNPs can significantly enhance the excitation of fluorescent dyes when the SPR of AuNPs overlaps with the absorption and emission spectra of fluorophores.[136] This phenomenon is called 'plasmon-enhanced fluorescence (PEF)', which was discovered shortly after the emergence of SERS.[137] The key to PEF is the distance between the AuNPs and fluorophores. AuNPs can enhance the fluorescence intensity of dyes only if the separation distance is appropriate (~5 nm). The fluorescence is unchanged if the separation distance is too large (>20 nm), whereas the fluorescence is quenched if the separation distance is very short (<2 nm).[138] PEF allows us to study weak fluorescence emission, even at the single molecule level. For example, Moerner *et al.* reported that the single-molecule fluorescence could be enhanced by gold bowtie nanoantennas by 1340-fold.[139] Khatua and coworkers used AuNR to achieve single-molecule fluorescence enhancement of a weak emitter, crystal violet, by a factor of 1000.[140] These findings are especially helpful to advance super-resolution fluorescence imaging. Jeynes *et al.* demonstrated AuNP-based DNA point accumulation for imaging in nanoscale topography (DNA-PAINT) to measure the nanoscale dimensions of individual telomeres in human cells.[141] The technique utilized an imaging probe composed of AuNPs and fluorescence capabilities, in combination with direct stochastic optical reconstruction microscopy (dSTORM) imaging and X-ray fluorescence microscopy, achieving an unprecedented spatial resolution of 5 nm.

Gold nanoclusters (AuNCls) were recently discovered to exhibit strong intrinsic fluorescence (in the visible and NIR region) that is highly photostable. AuNCls are AuNPs with diameters that are smaller than 2–3 nm, composed of several to hundreds of gold atoms. Because of their small sizes, AuNCls do not support the SPR effect. The intrinsic fluorescence of AuNCls can be directly used for both *in vitro* and *in vivo* imaging studies. Venkatesh and coworkers visualized the accumulation of 8-mercapto-9-propyladenine capped green AuNCls (emission at 510 nm) in cell nuclei.[142] Similarly, Wang *et al.* demonstrated

 

nuclear staining with tripeptide (Lys–Cys-–Lys) stabilized red AuNCls (emission at 680 nm).[143] Further, the intracellular accumulation and immune responses of AuNCls with different ligands were studied by Fernández and coworkers.[144] Chandirasekar *et al.*[145] and Zhang *et al.*[146] have employed AuNCls for *in vivo* fluorescent imaging of zebrafish embryos and implanted tumor in a mouse model, respectively. Their studies show that AuNCls have no toxicity on developing embryos but have remarkable penetration and retention in tumors.

In addition to PEF and intrinsic fluorescence, AuNPs can be directly used for two-photon (TP) and multi-photon (MP) imaging, which allow for greater tissue penetration and are suitable for *in vivo* imaging. The excitation light sources of TP and MP imaging are usually high intensity lasers, and therefore AuNPs are advantageous than organic fluorophores due to their high photostability. In addition, the two-photon absorption coefficient of AuNPs can be as high as 100-fold greater than that of organic fluorophores.[147] *In vivo* imaging study found that the two-photon fluorescent signal produced by a single AuNR in mouse ear blood vessels is 58 times stronger than that from a single rhodamine molecule.[148] Another study shows that AuNR-labeled cancer cells exhibit three orders of magnitude higher TP fluorescence intensity than the autofluorescence intensity from unlabeled cancer cells.[147] Besides AuNR, AuNSt also show strong TP fluorescent signals both *in vitro* and *in vivo*, due to their SPR in the NIR region.[149] Gao compared the TP signals of five different types of AuNPs with similar sizes: nanospheres, nanocubes, nanotriangles, AuNR, and AuNSt and found that the TP signal intensity increases in the order of nanospheres, nanocubes, nanotriangles, AuNR and AuNSt. The TP fluorescence intensity of AuNSt is 50 000-fold greater than that of gold nanospheres.[150]

## 5. Conclusions and perspectives

The unique and highly tunable optical properties of AuNPs have shown enormous potential in the development of state-of-the-art biosensing and bioimaging techniques. AuNP-based optical biosensors have great potential to be used as point-of-care devices due to their non-invasiveness, high sensitivity and highly reliable analytical results. Various Au nanostructure-based contrast agents have emerged for many optical imaging techniques including DFIC, OCT, PA, PT, Raman spectroscopy and fluorescence microscopy (Table 1). These novel imaging techniques allow precise imaging of cellular and molecular biomarkers with high resolution. Although proof-of-concept research papers of AuNP-based optical biosensors and bioimaging are increasing every year, these techniques still have a long way to go towards commercial and clinical applications. For biosensing, efforts should be made for high throughput and multiplexed identification of biomarkers. Multi-technology combination is another approach that can be adopted to improve the performance of sensing devices. The integration of AuNP-based optical sensing platforms with smartphones, portable, wearable and implantable devices is a future trend of exploration. More research is needed in manufacturing AuNPs with large scale and long-term stability under various environmental conditions. In addition to this, full attention is required in improving the analytical performance of biosensors by preventing non-specific adsorption of biomolecules onto AuNPs and shortening the analysis time. For biomedical imaging, more thorough research needs to be conducted to study the biodistribution, clearance pathways and long-term toxicity of AuNPs with different geometries and dimensions. In addition, better targeting agents and targeting strategies are needed to improve the molecular imaging specificity. The development of AuNP composites/hybrids with other nanomaterials is an exciting area that needs to be further explored as it may open new avenues of research and applications. For instance, composites of AuNPs with graphene, metal oxide nanoparticles and other two-dimensional nanomaterials have been explored to enhance optical biosensing performances.[151–154] A nanoparticle with a gold core, Raman active layer, silica shell and Gd coating was developed to achieve triple-modality imaging, which combines MRI, PA and Raman imaging.[155] In the near future, we envision that there will be tremendous growth in developing multifunctional AuNPs and AuNP-based nanohybrids for multi-analyte sensing and multi-modality imaging.

## Conflicts of interest

The authors declare no conflict of interest.

## Acknowledgements

NR, MW, and ON gratefully acknowledge the financial support and funding from the European Union's Horizon 2020 research and innovation program under the Marie Skłodowska-Curie grant agreement No. H2020-MSCA-ITN-2018-813680. NR wants to thank Prof. M. Hasanzadeh for valuable discussions. SS, CMP, RKG and BDM thank Prof. Yogesh Singh, Vice-Chancellor, Delhi Technological University, for his interest in this work. SS is thankful to CSIR, India, for the award of RA. CMP acknowledges the Department of Science and Technology, New Delhi, India, for the DST-INSPIRE Faculty Award (DST/INSPIRE/04/2015/000932). B. D. M. thanks the Science & Engineering Research Board (Government of India) for the award of a Distinguished Fellowship (SB/DF/011/2019). A. d. l. Z. would like to thank the Damon Runyon Cancer Research Foundation (DFS# 06-13), Claire Giannini Fund, the Susan G. Komen Breast Cancer Foundation (SAB15-00003), the Mary Kay Foundation (017-14), the Skippy Frank Foundation, the Donald E. and Delia B. Baxter Foundation, and a seed grant from the Center for Cancer Nanotechnology Excellence and Translation (CCNE-T; NIH-NCI U54CA151459). A. d. l. Z. is a Chan Zuckerberg Biohub investigator and a Pew-Stewart Scholar for Cancer Research supported by The Pew Charitable Trusts and The Alexander and Margaret Stewart Trust.

## References

1 T. Shimizu, T. Teranishi, S. Hasegawa and M. Miyake, Size Evolution of Alkanethiol-Protected Gold Nanoparticles by

Heat Treatment in the Solid State, *J. Phys. Chem. B*, 2003, **107**(12), 2719–2724.

2 Y.-S. Chen, Y. Zhao, S. J. Yoon, S. S. Gambhir and S. Emelianov, Miniature Gold Nanorods for Photoacoustic Molecular Imaging in the Second Near-Infrared Optical Window, *Nat. Nanotechnol.*, 2019, **14**(5), 465–472.

3 O. Liba, E. D. SoRelle, D. Sen and A. de la Zerda, Contrast-Enhanced Optical Coherence Tomography with Picomolar Sensitivity for Functional *In Vivo* Imaging, *Sci. Rep.*, 2016, **6**(1), 23337.

4 E. D. SoRelle, O. Liba, Z. Hussain, M. Gambhir and A. De La Zerda, Biofunctionalization of Large Gold Nanorods Realizes Ultrahigh-Sensitivity Optical Imaging Agents, *Langmuir*, 2015, **31**(45), 12339–12347.

5 A. Agrawal, S. Huang, A. Wei Haw Lin, M.-H. Lee, J. K. Barton, R. A. Drezek and T. J. Pfefer, Quantitative Evaluation of Optical Coherence Tomography Signal Enhancement with Gold Nanoshells, *J. Biomed. Opt.*, 2006, **11**(4), 041121.

6 A. M. Gobin, M. H. Lee, N. J. Halas, W. D. James, R. A. Drezek and J. L. West, Near-Infrared Resonant Nanoshells for Combined Optical Imaging and Photothermal Cancer Therapy, *Nano Lett.*, 2007, **7**(7), 1929–1934.

7 J. C. Y. Kah, M. Olivo, T. H. Chow, K. S. Song, K. Z. Y. Koh, S. Mhaisalkar and C. J. R. Sheppard, Control of Optical Contrast Using Gold Nanoshells for Optical Coherence Tomography Imaging of Mouse Xenograft Tumor Model *In Vivo*, *J. Biomed. Opt.*, 2009, **14**(5), 054015.

8 E. V. Zagaynova, M. V. Shirmanova, M. Y. Kirillin, B. N. Khlebtsov, A. G. Orlova, I. V. Balalaeva, M. A. Sirotkina, M. L. Bugrova, P. D. Agrba and V. A. Kamensky, Contrasting Properties of Gold Nanoparticles for Optical Coherence Tomography: Phantom, *In Vivo* Studies and Monte Carlo Simulation, *Phys. Med. Biol.*, 2008, **53**(18), 4995–5009.

9 M. Kirillin, M. Shirmanova, M. Sirotkina, M. Bugrova, B. Khlebtsov and E. Zagaynova, Contrasting Properties of Gold Nanoshells and Titanium Dioxide Nanoparticles for Optical Coherence Tomography Imaging of Skin: Monte Carlo Simulations and *In Vivo* Study, *J. Biomed. Opt.*, 2009, **14**(2), 021017.

10 J. Hu, F. Sanz-Rodríguez, F. Rivero, E. M. Rodríguez, R. A. Torres, D. H. Ortgies, J. G. Solé, F. Alfonso and D. Jaque, Gold Nanoshells: Contrast Agents for Cell Imaging by Cardiovascular Optical Coherence Tomography, *Nano Res.*, 2018, **11**(2), 676–685.

11 W. Lu, Q. Huang, G. Ku, X. Wen, M. Zhou, D. Guzatov, P. Brecht, R. Su, A. Oraevsky, L. V. Wang, *et al.*, Photoacoustic Imaging of Living Mouse Brain Vasculature Using Hollow Gold Nanospheres, *Biomaterials*, 2010, **31**(9), 2617–2626.

12 M.-L. Li, J. C. Wang, J. A. Schwartz, K. L. Gill-Sharp, G. Stoica and L. V. Wang, *In Vivo* Photoacoustic Microscopy of Nanoshell Extravasation from Solid Tumor Vasculature, *J. Biomed. Opt.*, 2009, **14**(1), 010507.

13 Y. Huang, A. R. Ferhan, Y. Gao, A. Dandapat and D.-H. Kim, High-Yield Synthesis of Triangular Gold Nanoplates with Improved Shape Uniformity, Tunable Edge Length and Thickness, *Nanoscale*, 2014, **6**(12), 6496–6500.

14 P. Si, E. Yuan, O. Liba, Y. Winetraub, S. Yousefi, E. D. SoRelle, D. W. Yecies, R. Dutta and A. de la Zerda, Gold Nanoprisms as Optical Coherence Tomography Contrast Agents in the Second Near-Infrared Window for Enhanced Angiography in Live Animals, *ACS Nano*, 2018, **12**(12), 11986–11994.

15 X. Jiang, P. Tang, P. Gao, Y. S. Zhang, C. Yi and J. Zhou, Gold Nanoprobe-Enabled Three-Dimensional Ozone Imaging by Optical Coherence Tomography, *Anal. Chem.*, 2017, **89**(4), 2561–2568.

16 C. M. Sweeney, C. L. Stender, C. L. Nehl, W. Hasan, K. L. Shuford and T. W. Odom, Optical Properties of Tipless Gold Nanopyramids, *Small*, 2011, **7**(14), 2032–2036.

17 D. Chateau, A. Liotta, F. Vadcard, J. R. G. Navarro, F. Chaput, J. Lermé, F. Lerouge and S. Parola, From Gold Nanobipyramids to Nanojavelins for a Precise Tuning of the Plasmon Resonance to the Infrared Wavelengths: Experimental and Theoretical Aspects, *Nanoscale*, 2015, **7**(5), 1934–1943.

18 P. Si, S. Shevidi, E. Yuan, K. Yuan, Z. Lautman, S. S. Jeffrey, G. W. Sledge and A. de la Zerda, Gold Nanobipyramids as Second Near Infrared Optical Coherence Tomography Contrast Agents for *In Vivo* Multiplexing Studies, *Nano Lett.*, 2020, **20**(1), 101–108.

19 E. Yuan, P. Si, Y. Winetraub, S. Shevidi and A. de la Zerda, A Spectral Demixing Model for Triplex *In Vivo* Imaging of Optical Coherence Tomography Contrast Agents, *ACS Photonics*, 2020, **7**(4), 893–900.

20 H. Cang, T. Sun, Z.-Y. Li, J. Chen, B. J. Wiley, Y. Xia and X. Li, Gold Nanocages as Contrast Agents for Spectroscopic Optical Coherence Tomography, *Opt. Lett.*, 2005, **30**(22), 3048.

21 H. B. Song, J. S. Wi, D. H. Jo, J. H. Kim, S. W. Lee, T. G. Lee and J. H. Kim, Intraocular Application of Gold Nanodisks Optically Tuned for Optical Coherence Tomography: Inhibitory Effect on Retinal Neovascularization without Unbearable Toxicity, *Nanomedicine*, 2017, **13**(6), 1901–1911.

22 J. S. Wi, J. Park, H. Kang, D. Jung, S. W. Lee and T. G. Lee, Stacked Gold Nanodisks for Bimodal Photoacoustic and Optical Coherence Imaging, *ACS Nano*, 2017, **11**(6), 6225–6232.

23 X. Yang, S. E. Skrabalak, Z. Y. Li, Y. Xia and L. V. Wang, Photoacoustic Tomography of a Rat Cerebral Cortex *In Vivo* with Au Nanocages as an Optical Contrast Agent, *Nano Lett.*, 2007, **7**(12), 3798–3802.

24 K. H. Song, C. Kim, C. M. Cobley, Y. Xia and L. V. Wang, Near-Infrared Gold Nanocages as a New Class of Tracers for Photoacoustic Sentinel Lymph Node Mapping on a Rat Model, *Nano Lett.*, 2009, **9**(1), 183–188.

25 Y. Xia, W. Li, C. M. Cobley, J. Chen, X. Xia, Q. Zhang, M. Yang, E. C. Cho and P. K. Brown, Gold Nanocages: From Synthesis to Theranostic Applications, *Acc. Chem. Res.*, 2011, **44**(10), 914–924.

 

26 C.-K. Lee, H.-Y. Tseng, C.-Y. Lee, S.-Y. Wu, T.-T. Chi, K.-M. Yang, H.-Y. E. Chou, M.-T. Tsai, J.-Y. Wang, Y.-W. Kiang, *et al.*, Characterizing the Localized Surface Plasmon Resonance Behaviors of Au Nanorings and Tracking Their Diffusion in Bio-Tissue with Optical Coherence Tomography, *Biomed. Opt. Express*, 2010, **1**(4), 1060–1073.

27 E. M. Larsson, J. Alegret, M. Käll and D. S. Sutherland, Sensing Characteristics of NIR Localized Surface Plasmon Resonances in Gold Nanorings, *Nano Lett.*, 2007, **7**(5), 1256–1263.

28 H. Y. Tseng, C. K. Lee, S. Y. Wu, T. T. Chi, K. M. Yang, J. Y. Wang, Y. W. Kiang, C. C. Yang, M. T. Tsai, Y. C. Wu, *et al.*, Au Nanorings for Enhancing Absorption and Backscattering Monitored with Optical Coherence Tomography, *Nanotechnology*, 2010, **21**(29).

29 T. H. Chow, Y. Lai, X. Cui, W. Lu, X. Zhuo and J. Wang, Colloidal Gold Nanorings and Their Plasmon Coupling with Gold Nanospheres, *Small*, 2019, **15**(35), 1902608.

30 H. B. Song, J. S. Wi, D. H. Jo, J. H. Kim, S. W. Lee, T. G. Lee and J. H. Kim, Intraocular Application of Gold Nanodisks Optically Tuned for Optical Coherence Tomography: Inhibitory Effect on Retinal Neovascularization without Unbearable Toxicity, *Nanomedicine*, 2017, **13**(6), 1901–1911.

31 Y. C. Ou, X. Wen, C. A. Johnson, D. Shae, O. D. Ayala, J. A. Webb, E. C. Lin, R. C. Delapp, K. L. Boyd, A. Richmond, *et al.*, Multimodal Multiplexed Immunoimaging with Nanostars to Detect Multiple Immunomarkers and Monitor Response to Immunotherapies, *ACS Nano*, 2020, **14**(1), 651–663.

32 Y.-C. Ou, J. A. Webb, C. M. O'Brien, I. J. Pence, E. C. Lin, E. P. Paul, D. Cole, S.-H. Ou, M. Lapierre-Landry, R. C. DeLapp, *et al.*, Diagnosis of Immunomarkers *In Vivo* via Multiplexed Surface Enhanced Raman Spectroscopy with Gold Nanostars, *Nanoscale*, 2018, **10**(27), 13092–13105.

33 H. Wang, D. W. Brandl, F. Le, P. Nordlander and N. J. Halas, Nanorice: A Hybrid Plasmonic Nanostructure, *Nano Lett.*, 2006, **6**(4), 827–832.

34 J. Ye, P. Van Dorpe, W. Van Roy, G. Borghs and G. Maes, Fabrication, Characterization , and Optical Properties of Gold Nanobowl Submonolayer Structures, *Langmuir*, 2009, **13**, 1822–1827.

35 R. Bukasov and J. S. Shumaker-Parry, Highly Tunable Infrared Extinction Properties of Gold Nanocrescents, *Nano Lett.*, 2007, **7**(5), 1113–1118.

36 Y. Lu, G. L. Liu, J. Kim, Y. X. Mejia and L. P. Lee, Nanophotonic Crescent Moon Structures with Sharp Edge for Ultrasensitive Biomolecular Detection by Local Electromagnetic Field Enhancement Effect, *Nano Lett.*, 2005, **5**(1), 119–124.

37 P. Singh, SPR Biosensors: Historical Perspectives and Current Challenges, *Sens. Actuators, B*, 2016, **229**, 110–130.

38 C. Sönnichsen, B. M. Reinhard, J. Liphardt and A. P. Alivisatos, A Molecular Ruler Based on Plasmon Coupling of Single Gold and Silver Nanoparticles, *Nat. Biotechnol.*, 2005, **23**(6), 741–745.

39 P. K. Jain, S. Eustis and M. A. El-Sayed, Plasmon Coupling in Nanorod Assemblies: Optical Absorption, Discrete Dipole Approximation Simulation, and Exciton-Coupling Model, *J. Phys. Chem. B*, 2006, **110**(37), 18243–18253.

40 L. Qin, G. Zeng, C. Lai, D. Huang, P. Xu, C. Zhang, M. Cheng, X. Liu, S. Liu and B. Li, "Gold Rush" in Modern Science: Fabrication Strategies and Typical Advanced Applications of Gold Nanoparticles in Sensing, *Coord. Chem. Rev.*, 2018, **359**, 1–31.

41 M. Shellaiah, T. Simon, P. Venkatesan, K. W. Sun, F.-H. Ko and S.-P. Wu, Nanodiamonds Conjugated to Gold Nanoparticles for Colorimetric Detection of Clenbuterol and Chromium(III) in Urine, *Microchim. Acta*, 2018, **185**(1), 74.

42 L. Zheng, G. Cai, S. Wang, M. Liao, Y. Li and J. Lin, A Microfluidic Colorimetric Biosensor for Rapid Detection of Escherichia Coli O157: H7 Using Gold Nanoparticle Aggregation and Smart Phone Imaging, *Biosens. Bioelectron.*, 2019, **124**, 143–149.

43 R. Rajamanikandan, A. D. Lakshmi and M. Ilanchelian, Smart Phone Assisted, Rapid, Simplistic, Straightforward and Sensitive Biosensing of Cysteine over Other Essential Amino Acids by β-Cyclodextrin Functionalized Gold Nanoparticles as a Colorimetric Probe, *New J. Chem.*, 2020, **44**(28), 12169–12177.

44 H. Aldewachi, T. Chalati, M. N. Woodroofe, N. Bricklebank, B. Sharrack and P. Gardiner, Gold Nanoparticle-Based Colorimetric Biosensors, *Nanoscale*, 2018, **10**(1), 18–33.

45 T. Yang, Z. Luo, Y. Tian, C. Qian and Y. Duan, Design Strategies of AuNPs-Based Nucleic Acid Colorimetric Biosensors, *TrAC, Trends Anal. Chem.*, 2019, 115795.

46 R. Elghanian, J. J. Storhoff, R. C. Mucic, R. L. Letsinger and C. A. Mirkin, Selective Colorimetric Detection of Polynucleotides Based on the Distance-Dependent Optical Properties of Gold Nanoparticles, *Science*, 1997, **277**(5329), 1078–1081.

47 J. J. Storhoff, R. Elghanian, R. C. Mucic, C. A. Mirkin and R. L. Letsinger, One-Pot Colorimetric Differentiation of Polynucleotides with Single Base Imperfections Using Gold Nanoparticle Probes, *J. Am. Chem. Soc.*, 1998, **120**(9), 1959–1964.

48 T. A. Taton, G. Lu and C. A. Mirkin, Two-Color Labeling of Oligonucleotide Arrays via Size-Selective Scattering of Nanoparticle Probes, *J. Am. Chem. Soc.*, 2001, **123**(21), 5164–5165.

49 M.-P. N. Bui, S. Ahmed and A. Abbas, Single-Digit Pathogen and Attomolar Detection with the Naked Eye Using Liposome-Amplified Plasmonic Immunoassay, *Nano Lett.*, 2015, **15**(9), 6239–6246.

50 B. Li, X. Li, Y. Dong, B. Wang, D. Li, Y. Shi and Y. Wu, Colorimetric Sensor Array Based on Gold Nanoparticles with Diverse Surface Charges for Microorganisms Identification, *Anal. Chem.*, 2017, **89**(20), 10639–10643.

51 Q. You, X. Zhang, F.-G. Wu and Y. Chen, Colorimetric and Test Stripe-Based Assay of Bacteria by Using Vancomycin-Modified Gold Nanoparticles, *Sens. Actuators, B*, 2019, **281**, 408–414.

52 M. Matsishin, A. Rachkov, A. Lopatynskyi, V. Chegel, A. Soldatkin and A. El'Skaya, Selective Amplification of SPR Biosensor Signal for Recognition of Rpob Gene Fragments by Use of Gold Nanoparticles Modified by Thiolated DNA, *Nanoscale Res. Lett.*, 2017, **12**(1), 1–6.

53 G. J. Nusz, S. M. Marinakos, A. C. Curry, A. Dahlin, F. Hook, A. Wax and A. Chilkoti, Label-Free Plasmonic Detection of Biomolecular Binding by a Single Gold Nanorod, *Anal. Chem.*, 2008, **80**(4), 984–989.

54 S. M. Marinakos, S. Chen and A. Chilkoti, Plasmonic Detection of a Model Analyte in Serum by a Gold Nanorod Sensor, *Anal. Chem.*, 2007, **79**(14), 5278–5283.

55 K. M. Mayer and J. H. Hafner, Localized Surface Plasmon Resonance Sensors, *Chem. Rev.*, 2011, **111**(6), 3828–3857.

56 H. Vaisocherová-Lísalová, I. Víšová, M. L. Ermini, T. Špringer, X. C. Song, J. Mrázek, J. Lamačová, N. S. Lynn Jr, P. Šedivák and J. Homola, Low-Fouling Surface Plasmon Resonance Biosensor for Multi-Step Detection of Foodborne Bacterial Pathogens in Complex Food Samples, *Biosens. Bioelectron.*, 2016, **80**, 84–90.

57 J. Zhou, C. Zhang, X. Zhang, C. Lu, T. Ming, Y. Li and X. Su, Immunomagnetic Separation-Based Nanogold Enhanced Surface Plasmon Resonance and Colloidal Gold Test Strips for Rapid Detection of *Vibrio parahaemolyticus*, *Arch. Microbiol.*, 2020, 1–9.

58 J. Yguerabide and E. E. Yguerabide, Light-Scattering Submicroscopic Particles as Highly Fluorescent Analogs and Their Use as Tracer Labels in Clinical and Biological Applications I. Theory, *Anal. Biochem.*, 1998, **262**(2), 137–156.

59 P. K. Jain, K. S. Lee, I. H. El-Sayed and M. A. El-Sayed, Calculated Absorption and Scattering Properties of Gold Nanoparticles of Different Size, Shape, and Composition: Applications in Biological Imaging and Biomedicine, *J. Phys. Chem. B*, 2006, **110**(14), 7238–7248.

60 J. Yguerabide and E. E. Yguerabide, Light-Scattering Submicroscopic Particles as Highly Fluorescent Analogs and Their Use as Tracer Labels in Clinical and Biological Applications, *Anal. Biochem.*, 1998, **262**(2), 157–176.

61 C. Loo, L. Hirsch, M.-H. Lee, E. Chang, J. West, N. Halas and R. Drezek, Gold Nanoshell Bioconjugates for Molecular Imaging in Living Cells, *Opt. Lett.*, 2005, **30**(9), 1012–1014.

62 C. Loo, A. Lowery, N. Halas, J. West and R. Drezek, Immunotargeted Nanoshells for Integrated Cancer Imaging and Therapy, *Nano Lett.*, 2005, **5**(4), 709–711.

63 N. Chanda, R. Shukla, K. V. Katti and R. Kannan, Gastrin Releasing Protein Receptor Specific Gold Nanorods: Breast and Prostate Tumor Avid Nanovectors for Molecular Imaging, *Nano Lett.*, 2009, **9**(5), 1798–1805.

64 M. P. Melancon, W. Lu, Z. Yang, R. Zhang, Z. Cheng, A. M. Elliot, J. Stafford, T. Olson, J. Z. Zhang and C. Li, In Vitro and *In Vivo* Targeting of Hollow Gold Nanoshells Directed at Epidermal Growth Factor Receptor for Photothermal Ablation Therapy, *Mol. Cancer Ther.*, 2008, **7**(6), 1730–1709.

65 J. L. Li, L. Wang, X. Y. Liu, Z. P. Zhang, H. C. Guo, W. M. Liu and S. H. Tang, In Vitro Cancer Cell Imaging and Therapy Using Transferrin-Conjugated Gold Nanoparticles, *Cancer Lett.*, 2009, **274**(2), 319–326.

66 W. Qian, X. Huang, B. Kang and M. A. El-Sayed, Dark-Field Light Scattering Imaging of Living Cancer Cell Component from Birth through Division Using Bioconjugated Gold Nanoprobes, *J. Biomed. Opt.*, 2010, **15**(4), 046025.

67 X. Y. Wan, L. L. Zheng, P. F. Gao, X. X. Yang, C. M. Li, Y. F. Li and C. Z. Huang, Real-Time Light Scattering Tracking of Gold Nanoparticles-Bioconjugated Respiratory Syncytial Virus Infecting HEp-2 Cells, *Sci. Rep.*, 2014, **4**, 4529.

68 T. S. Troutman, J. K. Barton and M. Romanowski, Optical Coherence Tomography with Plasmon Resonant Nanorods of Gold, *Opt. Lett.*, 2007, **32**(11), 1438.

69 A. de la Zerda, S. Prabhulkar, V. L. Perez, M. Ruggeri, A. S. Paranjape, F. Habte, S. S. Gambhir and R. M. Awdeh, Optical Coherence Contrast Imaging Using Gold Nanorods in Living Mice Eyes, *Clin. Exp. Ophthalmol.*, 2015, **43**(4), 358–366.

70 Y. Winetraub, E. D. SoRelle, O. Liba and A. De La Zerda, Quantitative Contrast-Enhanced Optical Coherence Tomography, *Appl. Phys. Lett.*, 2016, **108**(2), 023702.

71 K. M. Ratheesh, P. Prabhathan, L. K. Seah and V. M. Murukeshan, Gold Nanorods with Higher Aspect Ratio as Potential Contrast Agent in Optical Coherence Tomography and for Photothermal Applications around 1300 nm Imaging Window, *Biomed. Phys. Eng. Express*, 2016, **2**(5), 055005.

72 D. Sen, E. D. SoRelle, O. Liba, R. Dalal, Y. M. Paulus, T.-W. Kim, D. M. Moshfeghi, A. de la Zerda, D. Sen, D. M. Moshfeghi, *et al.*, High-Resolution Contrast-Enhanced Optical Coherence Tomography in Mice Retinae, *J. Biomed. Opt.*, 2016, **21**(6), 066002.

73 N. Lippok, M. Villiger, A. Albanese, E. F. J. Meijer, K. Chung, T. P. Padera, S. N. Bhatia and B. E. Bouma, Depolarization Signatures Map Gold Nanorods within Biological Tissue, *Nat. Photonics*, 2017, **11**(9), 583–588.

74 E. D. Sorelle, D. W. Yecies, O. Liba, F. C. Bennett, C. M. Graef, R. Dutta, S. Mitra, L. M. Joubert, S. Cheshier, G. A. Grant, *et al.*, Spatiotemporal Tracking of Brain-Tumor-Associated Myeloid Cells *In Vivo* through Optical Coherence Tomography with Plasmonic Labeling and Speckle Modulation, *ACS Nano*, 2019, **13**(7), 7985–7995.

75 O. Bibikova, A. Popov, A. Bykov, A. Prilepskyii, M. Kinnunen, K. Kordas, V. Bogatyrev, N. Khlebtsov and V. Tuchin, Gold Nanostructures for OCT Imaging of Capillary Flow, *Proc. SPIE*, 2014, **9129**, 1–9.

76 X. Jiang, R. Liu, P. Tang, W. Li, H. Zhong, Z. Zhou and J. Zhou, Controllably Tuning the Near-Infrared Plasmonic Modes of Gold Nanoplates for Enhanced Optical Coherence Imaging and Photothermal Therapy, *RSC Adv.*, 2015, **5**, 80709–80718.

77 P. Tang, X. Jiang, Y. Wang, H. Chen, Y. S. Zhang, P. Gao, H. Wang, X. Li and J. Zhou, Plasmonic Nanoprobe of (Gold Triangular Nanoprism Core)/(Polyaniline Shell) for Real-Time Three-Dimensional pH Imaging of Anterior Chamber, *Anal. Chem.*, 2017, **89**(18), 9758–9766.

 

78 X. Ye, L. Jin, H. Caglayan, J. Chen, G. Xing and C. Zheng, Improved Size-Tunable Synthesis of Monodisperse Gold Nanorods through the Use of Aromatic Additives, *ACS Nano*, 2012, **3**, 2804–2817.

79 E. D. SoRelle, D. W. Yecies, O. Liba, F. C. Bennett, C. M. Graef, R. Dutta, S. Mitra, L.-M. Joubert, S. Cheshier, G. A. Grant, *et al.*, Spatiotemporal Tracking of Brain-Tumor-Associated Myeloid Cells *In Vivo* through Optical Coherence Tomography with Plasmonic Labeling and Speckle Modulation, *ACS Nano*, 2019, **13**(7), 7985–7995.

80 R. Dutta, O. Liba, E. D. Sorelle, Y. Winetraub, V. C. Ramani, S. S. Jeffrey, G. W. Sledge and A. De La Zerda, Real-Time Detection of Circulating Tumor Cells in Living Animals Using Functionalized Large Gold Nanorods, *Nano Lett.*, 2019, **19**(4), 2334–2342.

81 D. Boyer, P. Tamarat, A. Maali, B. Lounis and M. Orrit, Photothermal Imaging of Nanometer-Sized Metal Particles among Scatterers, *Science*, 2002, **297**(5584), 1160–1163.

82 S. Berciaud, L. Cognet, P. Tamarat and B. Lounis, Observation of Intrinsic Size Effects in the Optical Response of Individual Gold Nanoparticles, *Nano Lett.*, 2005, **5**(3), 515–518.

83 V. P. Zharov and D. O. Lapotko, Photothermal Imaging of Nanoparticles and Cells, *IEEE J. Sel. Top. Quantum Electron.*, 2005, **11**(4), 733–751.

84 V. P. Zharov, E. I. Galanzha and V. V. Tuchin, Photothermal Flow Cytometry In Vitro for Detection and Imaging of Individual Moving Cells, *Cytometry, Part A*, 2007, **71**(4), 191–206.

85 V. P. Zharov, E. I. Galanzha and V. V. Tuchin, Photothermal Image Flow Cytometry *In Vivo*, *Opt. Lett.*, 2005, **30**(6), 628–630.

86 E. I. Galanzha, J. W. Kim and V. P. Zharov, Nanotechnology-Based Molecular Photoacoustic and Photothermal Flow Cytometry Platform for *In Vivo* Detection and Killing of Circulating Cancer Stem Cells, *J. Biophotonics*, 2009, **2**(12), 725–735.

87 J. W. Kim, E. I. Galanzha, E. V. Shashkov, H. M. Moon and V. P. Zharov, Golden Carbon Nanotubes as Multimodal Photoacoustic and Photothermal High-Contrast Molecular Agents, *Nat. Nanotechnol.*, 2009, **4**, 688–694.

88 D. A. Nedosekin, E. I. Galanzha, E. Dervishi, A. S. Biris and V. P. Zharov, Super-Resolution Nonlinear Photothermal Microscopy, *Small*, 2014, **10**(1), 135–142.

89 S. P. Mattison, W. Kim, J. Park and B. E. Applegate, Molecular Imaging in Optical Coherence Tomography, *Curr. Mol. Imaging*, 2015, **3**(2), 88–105.

90 M. C. Skala, M. J. Crow, A. Wax and J. A. Izatt, Photothermal Optical Coherence Tomography of Epidermal Growth Factor Receptor in Live Cells Using Immunotargeted Gold Nanospheres, *Nano Lett.*, 2008, **8**(10), 3461–3467.

91 C. Zhou, T.-H. Tsai, D. C. Adler, H.-C. Lee, D. W. Cohen, A. Mondelblatt, Y. Wang, J. L. Connolly and J. G. Fujimoto, Photothermal Optical Coherence Tomography in Ex Vivo Human Breast Tissues Using Gold Nanoshells, *Opt. Lett.*, 2010, **35**(5), 700.

92 J. M. Tucker-Schwartz, T. A. Meyer, C. A. Patil, C. L. Duvall and M. C. Skala, *In Vivo* Photothermal Optical Coherence Tomography of Gold Nanorod Contrast Agents, *Biomed. Opt. Express*, 2012, **3**(11), 2881.

93 J. M. Tucker-Schwartz, K. R. Beavers, W. W. Sit, A. T. Shah, C. L. Duvall and M. C. Skala, *In Vivo* Imaging of Nanoparticle Delivery and Tumor Microvasculature with Multimodal Optical Coherence Tomography, *Biomed. Opt. Express*, 2014, **5**(6), 1731.

94 M. Lapierre-Landry, A. Y. Gordon, J. S. Penn and M. C. Skala, *In Vivo* Photothermal Optical Coherence Tomography of Endogenous and Exogenous Contrast Agents in the Eye, *Sci. Rep.*, 2017, **7**(1), 1–9.

95 A. Y. Gordon, M. Lapierre-Landry, M. C. Skala and J. S. Penn, Photothermal Optical Coherence Tomography of Anti-Angiogenic Treatment in the Mouse Retina Using Gold Nanorods as Contrast Agents, *Transl. Vis. Sci. Technol.*, 2019, **8**(3).

96 V. Sebastián, S.-K. Lee, C. Zhou, M. F. Kraus, J. G. Fujimoto and K. F. Jensen, One-Step Continuous Synthesis of Biocompatible Gold Nanorods for Optical Coherence Tomography, *Chem. Commun.*, 2012, **48**(53), 6654.

97 Y. Jung, R. Reif, Y. Zeng and R. K. Wang, Three-Dimensional High-Resolution Imaging of Gold Nanorods Uptake in Sentinel Lymph Nodes, *Nano Lett.*, 2011, **11**(7), 2938–2943.

98 Q. Zhang, N. Iwakuma, P. Sharma, B. M. Moudgil, C. Wu, J. McNeill, H. Jiang and S. R. Grobmyer, Gold Nanoparticles as a Contrast Agent for *In Vivo* Tumor Imaging with Photoacoustic Tomography, *Nanotechnology*, 2009, **20**(39), 395102.

99 M. Eghtedari, A. Oraevsky, J. A. Copland, N. A. Kotov, A. Conjusteau and M. Motamedi, High Sensitivity of *In Vivo* Detection of Gold Nanorods Using a Laser Optoacoustic Imaging System, *Nano Lett.*, 2007, **7**(7), 1914–1918.

100 A. Taruttis, E. Herzog, D. Razansky and V. Ntziachristos, Real-Time Imaging of Cardiovascular Dynamics and Circulating Gold Nanorods with Multispectral Optoacoustic Tomography, *Opt. Express*, 2010, **18**(19), 19592–19602.

101 P.-C. Li, C.-R. C. Wang, D.-B. Shieh, C.-W. Wei, C.-K. Liao, C. Poe, S. Jhan, A.-A. Ding and Y.-N. Wu, *In Vivo* Photoacoustic Molecular Imaging with Simultaneous Multiple Selective Targeting Using Antibody-Conjugated Gold Nanorods, *Opt. Express*, 2008, **16**(23), 18605–18615.

102 C. L. Bayer, Y.-S. Chen, S. Kim, S. Mallidi, K. Sokolov and S. Emelianov, Multiplex Photoacoustic Molecular Imaging Using Targeted Silica-Coated Gold Nanorods, *Biomed. Opt. Express*, 2011, **2**(7), 1828–1835.

103 J. V. Jokerst, M. Thangaraj, P. J. Kempen, R. Sinclair and S. S. Gambhir, Photoacoustic Imaging of Mesenchymal Stem Cells in Living Mice via Silica-Coated Gold Nanorods, *ACS Nano*, 2012, **6**(7), 5920–5930.

104 S. Yang, F. Ye and D. Xing, Intracellular Label-Free Gold Nanorods Imaging with Photoacoustic Microscopy, *Opt. Express*, 2012, **20**(9), 10370–10375.

105 C. Kim, H. M. Song, X. Cai, J. Yao, A. Wei and L. V. Wang, *In Vivo* Photoacoustic Mapping of Lymphatic Systems with Plasmon-Resonant Nanostars, *J. Mater. Chem.*, 2011, **21**, 2841–2844.

106 S. Laing, L. E. Jamieson, K. Faulds and D. Graham, Surface-Enhanced Raman Spectroscopy for *In Vivo* Biosensing, *Nat. Rev. Chem.*, 2017, **1**(8), 1–19.

107 X. Lu, Y. Huang, B. Liu, L. Zhang, L. Song, J. Zhang, A. Zhang and T. Chen, Light-Controlled Shrinkage of Large-Area Gold Nanoparticle Monolayer Film for Tunable SERS Activity, *Chem. Mater.*, 2018, **30**(6), 1989–1997.

108 S. Si, W. Liang, Y. Sun, J. Huang, W. Ma, Z. Liang, Q. Bao and L. Jiang, Facile Fabrication of High-Density Sub-1 nm Gaps from Au Nanoparticle Monolayers as Reproducible SERS Substrates, *Adv. Funct. Mater.*, 2016, **26**(44), 8137–8145.

109 L. Song, Y. Huang, Z. Nie and T. Chen, Macroscopic Two-Dimensional Monolayer Films of Gold Nanoparticles: Fabrication Strategies, Surface Engineering and Functional Applications, *Nanoscale*, 2020, **12**, 7433–7460.

110 H. Shao, H. Lin, Z. Guo, J. Lu, Y. Jia, M. Ye, F. Su, L. Niu, W. Kang, S. Wang, *et al.*, A Multiple Signal Amplification Sandwich-Type SERS Biosensor for Femtomolar Detection of miRNA, *Biosens. Bioelectron.*, 2019, **143**, 111616.

111 Q. Cheng, L. Song, H. Lin, Y. Yang, Y. Huang, F. Su and T. Chen, Free-Standing 2D Janus Gold Nanoparticles Monolayer Film with Tunable Bifacial Morphologies via the Asymmetric Growth at Air–Liquid Interface, *Langmuir*, 2020, **36**(1), 250–256.

112 X. Wang, N. Choi, Z. Cheng, J. Ko, L. Chen and J. Choo, Simultaneous Detection of Dual Nucleic Acids Using a SERS-Based Lateral Flow Assay Biosensor, *Anal. Chem.*, 2017, **89**(2), 1163–1169.

113 M. Fleischmann, P. J. Hendra and A. J. McQuillan, Raman spectra of pyridine adsorbed at a silver electrode, *Chem. Phys. Lett.*, 1974, **26**(2), 163–166.

114 Y. Li, H. J. Schluesener and S. Xu, Gold Nanoparticle-Based Biosensors, *Gold Bull.*, 2010, **43**(1), 29–41.

115 D. S. Kopitsyn, M. V. Gorbachevskii, E. A. Botchkova, M. A. Bychenko and A. A. Novikov, Identification of Bacteria by Surface-Enhanced Raman Spectra after Peroxide Treatment, *Appl. Biochem. Microbiol.*, 2019, **55**(1), 78–82.

116 A. H. H. Mevold, W.-W. Hsu, A. Hardiansyah, L.-Y. Huang, M.-C. Yang, T.-Y. Liu, T.-Y. Chan, K.-S. Wang, Y.-A. Su and R.-J. Jeng, Fabrication of Gold Nanoparticles/Graphene–PDDA Nanohybrids for Bio-Detection by SERS Nanotechnology, *Nanoscale Res. Lett.*, 2015, **10**(1), 1–7.

117 X. Ma, X. Xu, Y. Xia and Z. Wang, SERS Aptasensor for *Salmonella typhimurium* Detection Based on Spiny Gold Nanoparticles, *Food Control*, 2018, **84**, 232–237.

118 S. Harmsen, R. Huang, M. A. Wall, H. Karabeber, J. M. Samii, M. Spaliviero, J. R. White, S. Monette, R. O'Connor, K. L. Pitter, *et al.*, Surface-Enhanced Resonance Raman Scattering Nanostars for High-Precision Cancer Imaging, *Sci. Transl. Med.*, 2015, **7**(271), 271ra7.

119 T. Vo-Dinh, H. N. Wang and H. T. Ngo *Biomedical Photonics Handbook*, ed. T. Vo-Dinh, CRC Press, 2014.

120 G. L. Liu, Y. Lu, J. Kim, J. C. Doll and L. P. Lee, Magnetic Nanocrescents as Controllable Surface-Enhanced Raman Scattering Nanoprobes for Biomolecular Imaging, *Adv. Mater.*, 2005, **17**(22), 2683–2688.

121 G. W. Kim and J. W. Ha, Polarization- and Wavelength-Dependent Defocused Scattering Imaging of Single Gold Nanostars with Multiple Long Branches, *Photochem. Photobiol. Sci.*, 2019, **18**, 1430–1435.

122 G. H. Jeong, Y. W. Lee, M. Kim and S. W. Han, High-Yield Synthesis of Multi-Branched Gold Nanoparticles and Their Surface-Enhanced Raman Scattering Properties, *J. Colloid Interface Sci.*, 2009, **329**(1), 97–102.

123 O. M. Bakr, B. H. Wunsch and F. Stellacci, High-Yield Synthesis of Multi-Branched Urchin-Like Gold Nanoparticles, *Chem. Mater.*, 2006, **18**(14), 3297–3301.

124 Y. Kang, H. X. Gu and X. Zhang, A Self-Referenced Method for Determination of Patulin by Surface-Enhanced Raman Scattering Using Gold Nanobipyramids as the Substrate, *Anal. Methods*, 2019, **11**, 5142–5149.

125 S. Y. Lee, Y. Han, J. W. Hong and J. W. Ha, Single Gold Bipyramids with Sharp Tips as Sensitive Single Particle Orientation Sensors in Biological Studies, *Nanoscale*, 2017, **9**, 12060–12067.

126 A. A. Saeed, J. L. A. Sánchez, C. K. O'Sullivan and M. N. Abbas, DNA Biosensors Based on Gold Nanoparticles-Modified Graphene Oxide for the Detection of Breast Cancer Biomarkers for Early Diagnosis, *Bioelectrochemistry*, 2017, **118**, 91–99.

127 N. Elahi, M. Kamali, M. H. Baghersad and B. Amini, A Fluorescence Nano-Biosensors Immobilization on Iron (MNPs) and Gold (AuNPs) Nanoparticles for Detection of *Shigella* spp., *Mater. Sci. Eng., C*, 2019, **105**, 110113.

128 S. Xu, F. Zhang, L. Xu, X. Liu, P. Ma, Y. Sun, X. Wang and D. Song, A Fluorescence Resonance Energy Transfer Biosensor Based on Carbon Dots and Gold Nanoparticles for the Detection of Trypsin, *Sens. Actuators, B*, 2018, **273**, 1015–1021.

129 X. Fu, X. Fu, Q. Wang, L. Sheng, X. Huang, M. Ma and Z. Cai, Fluorescence Switch Biosensor Based on Quantum Dots and Gold Nanoparticles for Discriminative Detection of Lysozyme, *Int. J. Biol. Macromol.*, 2017, **103**, 1155–1161.

130 S. Barua, S. Gogoi and R. Khan, Fluorescence Biosensor Based on Gold–Carbon Dot Probe for Efficient Detection of Cholesterol, *Synth. Met.*, 2018, **244**, 92–98.

131 H. Zhang and Z. Jia, Development of Fluorescent FRET Probes for "Off–On" Detection of L-Cysteine Based on Gold Nanoparticles and Porous Silicon Nanoparticles in Ethanol Solution, *Sensors*, 2017, **17**(3), 520.

132 B. Jin, S. Wang, M. Lin, Y. Jin, S. Zhang, X. Cui, Y. Gong, A. Li, F. Xu and T. J. Lu, Upconversion Nanoparticles Based FRET Aptasensor for Rapid and Ultrasensitive Bacteria Detection, *Biosens. Bioelectron.*, 2017, **90**, 525–533.

 

133 W. Bai, Y. Wei, Y. Zhang, L. Bao and Y. Li, Label-Free and Amplified Electrogenerated Chemiluminescence Biosensing for the Detection of Thymine DNA Glycosylase Activity Using DNA-Functionalized Gold Nanoparticles Triggered Hybridization Chain Reaction, *Anal. Chim. Acta*, 2019, **1061**, 101–109.

134 A. Cui, J. Zhang, W. Bai, H. Sun, L. Bao, F. Ma and Y. Li, Signal-on Electrogenerated Chemiluminescence Biosensor for Ultrasensitive Detection of microRNA-21 Based on Isothermal Strand-Displacement Polymerase Reaction and Bridge DNA–Gold Nanoparticles, *Biosens. Bioelectron.*, 2019, **144**, 111664.

135 H. Zhang, Z. Wang, F. Wang, Y. Zhang, H. Wang and Y. Liu, In Situ Formation of Gold Nanoparticles Decorated $Ti_3C_2$ MXenes Nanoprobe for Highly Sensitive Electrogenerated Chemiluminescence Detection of Exosomes and Their Surface Proteins, *Anal. Chem.*, 2020, **92**(7), 5546–5553.

136 J. F. Li, C. Y. Li and R. F. Aroca, Plasmon-Enhanced Fluorescence Spectroscopy, *Chem. Soc. Rev.*, 2017, **46**, 3962–3979.

137 J. Gersten and A. Nitzan, Spectroscopic Properties of Molecules Interacting with Small Dielectric Particles, *J. Chem. Phys.*, 1981, **75**(3), 1139–1152.

138 Y. Wu, M. R. K. Ali, K. Chen, N. Fang and M. A. El-Sayed, Gold Nanoparticles in Biological Optical Imaging, *Nano Today*, 2019, 120–140.

139 A. Kinkhabwala, Z. Yu, S. Fan, Y. Avlasevich, K. Müllen and W. E. Moerner, Large Single-Molecule Fluorescence Enhancements Produced by a Bowtie Nanoantenna, *Nat. Photonics*, 2009, **3**(11), 654–657.

140 S. Khatua, P. M. R. Paulo, H. Yuan, A. Gupta, P. Zijlstra and M. Orrit, Resonant Plasmonic Enhancement of Single-Molecule Fluorescence by Individual Gold Nanorods, *ACS Nano*, 2014, **8**(5), 4440–4449.

141 J. C. G. Jeynes, K. Geraki, C. Jeynes, M. Zhaohong, A. A. Bettiol, E. Latorre, L. W. Harries and C. Soeller, Nanoscale Properties of Human Telomeres Measured with a Dual Purpose X-Ray Fluorescence and Super Resolution Microscopy Gold Nanoparticle Probe, *ACS Nano*, 2017, **11**(12), 12632–12640.

142 V. Venkatesh, A. Shukla, S. Sivakumar and S. Verma, Purine-Stabilized Green Fluorescent Gold Nanoclusters for Cell Nuclei Imaging Applications, *ACS Appl. Mater. Interfaces*, 2014, **6**(3), 2185–2191.

143 X. Wang, Y. Wang, H. He, X. Ma, Q. Chen, S. Zhang, B. Ge, S. Wang, W. M. Nau and F. Huang, Deep-Red Fluorescent Gold Nanoclusters for Nucleoli Staining: Real-Time Monitoring of the Nucleolar Dynamics in Reverse Transformation of Malignant Cells, *ACS Appl. Mater. Interfaces*, 2017, **9**(21), 17799–17806.

144 T. D. Fernández, J. R. Pearson, M. P. Leal, M. J. Torres, M. Blanca, C. Mayorga and X. Le Guével, Intracellular Accumulation and Immunological Properties of Fluorescent Gold Nanoclusters in Human Dendritic Cells, *Biomaterials*, 2015, **43**, 1–12.

145 S. Chandirasekar, C. Chandrasekaran, T. Muthukumara samyvel, G. Sudhandiran and N. Rajendiran, Biosurfactant Templated Quantum Sized Fluorescent Gold Nanoclusters for *In Vivo* Bioimaging in Zebrafish Embryos, *Colloids Surf., B*, 2016, **143**, 472–480.

146 C. Zhang, C. Li, Y. Liu, J. Zhang, C. Bao, S. Liang, Q. Wang, Y. Yang, H. Fu, K. Wang, *et al.*, Gold Nanoclusters-Based Nanoprobes for Simultaneous Fluorescence Imaging and Targeted Photodynamic Therapy with Superior Penetration and Retention Behavior in Tumors, *Adv. Funct. Mater.*, 2015, **25**(8), 1314–1325.

147 N. J. Durr, T. Larson, D. K. Smith, B. A. Korgel, K. Sokolov and A. Ben-Yakar, Two-Photon Luminescence Imaging of Cancer Cells Using Molecularly Targeted Gold Nanorods, *Nano Lett.*, 2007, **7**(4), 941–945.

148 H. Wang, T. B. Huff, D. A. Zweifel, W. He, P. S. Low, A. Wei and J. X. Cheng, In Vitro and *In Vivo* Two-Photon Luminescence Imaging of Single Gold Nanorods, *Proc. Natl. Acad. Sci. U. S. A.*, 2005, **102**(44), 15752–15756.

149 H. Yuan, C. G. Khoury, H. Hwang, C. M. Wilson, G. A. Grant and T. Vo-Dinh, Gold Nanostars: Surfactant-Free Synthesis, 3D Modelling, and Two-Photon Photoluminescence Imaging, *Nanotechnology*, 2012, **23**(7), 075102.

150 N. Gao, Y. Chen, L. Li, Z. Guan, T. Zhao, N. Zhou, P. Yuan, S. Q. Yao and Q. H. Xu, Shape-Dependent Two-Photon Photoluminescence of Single Gold Nanoparticles, *J. Phys. Chem. C*, 2014, **118**(25), 13904–13911.

151 I. Khalil, W. A. Yehye, N. M. Julkapli, S. Rahmati, A. A. I. Sina, W. J. Basirun and M. R. Johan, Graphene Oxide and Gold Nanoparticle Based Dual Platform with Short DNA Probe for the PCR Free DNA Biosensing Using Surface-Enhanced Raman Scattering, *Biosens. Bioelectron.*, 2019, **131**, 214–223.

152 X. Cao, Z. Xia, W. Yan, S. He, X. Xu, Z. Wei, Y. Ye and H. Zheng, Colorimetric Biosensing of Nopaline Synthase Terminator Using $Fe_3O_4$@Au and Hemin-Functionalized Reduced Graphene Oxide, *Anal. Biochem.*, 2020, **602**, 113798.

153 L. Xiao, A. Zhu, Q. Xu, Y. Chen, J. Xu and J. Weng, Colorimetric Biosensor for Detection of Cancer Biomarker by Au Nanoparticle-Decorated $Bi_2Se_3$ Nanosheets, *ACS Appl. Mater. Interfaces*, 2017, **9**(8), 6931–6940.

154 Z.-M. Li, X. Zhang, T. Pi, J. Bu, R.-H. Deng, B.-Z. Chi and X.-J. Zheng, Colorimetric Determination of the Activity of Methyltransferase Based on Nicking Enzyme Amplification and the Use of Gold Nanoparticles Conjugated to Graphene Oxide, *Microchim. Acta*, 2019, **186**(8), 594.

155 M. F. Kircher, A. De La Zerda, J. V. Jokerst, C. L. Zavaleta, P. J. Kempen, E. Mittra, K. Pitter, R. Huang, C. Campos, F. Habte, *et al.*, A Brain Tumor Molecular Imaging Strategy Using a New Triple-Modality MRI-Photoacoustic-Raman Nanoparticle, *Nat. Med.*, 2012, **18**(5), 829–834.

156 X. Huang, I. H. El-Sayed, W. Qian and M. A. El-Sayed, Cancer Cell Imaging and Photothermal Therapy in the Near-Infrared Region by Using Gold Nanorods, *J. Am. Chem. Soc.*, 2006, **128**(6), 2115–2120.

157 S. Oldenburg, R. Averitt, S. Westcott and N. Halas, Nanoengineering of Optical Resonances, *Chem. Phys. Lett.*, 1998, **288**(2–4), 243–247.

158 X. Huang, S. Neretina and M. A. El-Sayed, Gold Nanorods: From Synthesis and Properties to Biological and Biomedical Applications, *Adv. Mater.*, 2009, **21**(48), 4880–4910.

159 A. Guerrero-Martínez, S. Barbosa, I. Pastoriza-Santos and L. M. Liz-Marzán, Nanostars Shine Bright for You, *Curr. Opin. Colloid Interface Sci.*, 2011, **16**(2), 118–127.

160 J. Chen, J. M. McLellan, A. Siekkinen, Y. Xiong, Z.-Y. Li and Y. Xia, Facile Synthesis of Gold–Silver Nanocages with Controllable Pores on the Surface, *J. Am. Chem. Soc.*, 2006, **128**(46), 14776–14777.

161 X. Jiang, P. Tang, P. Gao, Y. S. Zhang, C. Yi and J. Zhou, Gold Nanoprobe-Enabled Three-Dimensional Ozone Imaging by Optical Coherence Tomography, *Anal. Chem.*, 2017, **89**(4), 2561–2568.

162 J. Henzie, E.-S. Kwak and T. W. Odom, Mesoscale Metallic Pyramids with Nanoscale Tips, *Nano Lett.*, 2005, **5**(7), 1199–1202.

163 M. I. Halawa, J. Lai and G. Xu, Gold Nanoclusters: Synthetic Strategies and Recent Advances in Fluorescent Sensing, *Materials Today Nano*, 2018, 9–27.